Evaluation and improvement of macroscopic yield criteria of porous media having a Drucker-Prager matrix

Wanqing Shen, Jian-Fu Shao, Z.B. Liu, A. Oueslati, G. de Saxcé

Version of Record: https://www.sciencedirect.com/science/article/pii/S0749641919304723
Manuscript_f883298132771d57584cc33fc44440d9

Evaluation and improvement of macroscopic yield criteria of porous media having a Drucker-Prager matrix

W.Q. Shen[a,b,*], J.F. Shao[a,b,*], Z.B. Liu[a]

[a] *Key Laboratory of Ministry of Education on Safe Mining of Deep Metal Mines, College of Resources and Civil Engineering, Northeastern University, Shenyang, 110819, China*
[b] *Univ. Lille, CNRS, Centrale Lille, FRE 2016 - LaMcube - Laboratoire de mécanique multiphysique et multiéchelle, F-59000, Lille, France*

Abstract

A large number of analytical strength criteria have been developed for porous materials having a Drucker-Prager solid matrix by using different up-scaling methods. A number of representative exisitng criteria are selected and summarized. These criteria are first evaluated and compared both analytically and numerically with new FEM solutions obtained in this work. A wide variety of new numerical results are then provided from finite element simulations to enlarge the comparisons. In particular, the strength under the pure shear condition is discussed and studied in depth, either numerically and theoretically. Based on these comparisons, a new improvement of the prediction of pure shear strength is established. With this improvement, we derive a new macroscopic strength criterion for the porous materials with a Drucker-Prager type solid matrix. The new criterion is validated against those numerical solutions for a wide range of porosity and frictional coefficient. The special case of a porous material with a von Mises type solid matrix is also studied with a good validation.

Keywords: Strength criterion, Micro-mechanics, Porosity, Drucker-Prager, Pressure sensitive materials

*Corresponding authors: jian-fu.shao@polytech-lille.fr, wanqing.shen@polytech-lille.fr

Nomenclature

a	Scalar
$\underline{a}$	Vector
$\boldsymbol{a}$	Second order tensor
$\mathbf{1}$	Second order unit tensor
$\boldsymbol{a}'$	Deviator of a second order tensor $\boldsymbol{a}$
a_m	Hydrostatic part of a second order tensor $\boldsymbol{a}$: $a_m = tr\boldsymbol{a}/3$
f	Micro porosity
α	Frictional parameter of the matrix
β	Dilatancy parameter of the matrix
$\boldsymbol{\sigma}$	Microscopic stress field
$\boldsymbol{\Sigma}$	Macroscopic stress field
σ_{eq}, Σ_{eq}	Micro and macro equivalent stress: $\sigma_{eq} = \sqrt{\frac{3}{2}\boldsymbol{\sigma}' : \boldsymbol{\sigma}'}$, $\Sigma_{eq} = \sqrt{\frac{3}{2}\boldsymbol{\Sigma}' : \boldsymbol{\Sigma}'}$
$\boldsymbol{d}$	Microscopic strain rate
$\boldsymbol{D}$	Macroscopic strain rate
d_{eq}	Equivalent strain: $d_{eq} = \sqrt{\frac{2}{3}\boldsymbol{d}' : \boldsymbol{d}'}$
$\pi(\boldsymbol{d})$	Support function of the mtrix
$\dot{\lambda}$	The plastic multiplier
$\dot{\Lambda}$	The Lagrange's multiplier
$\underline{v}$	Velocity field
σ_0	The strength of matrix in pure shear loading
.	Simple contraction of two tensors
:	Double contraction of two tensors
$\otimes$	Tensorial product

1. Introduction

In civil engineering and petroleum engineering, most materials are porous media with a high porosity. Elastic properties, plastic deformation and failure strength of porous materials are inherently affected by the porosity and the presence of fluid phases. Therefore, there are two main objectives in mechanics of porous media, which can be either separately or simultaneously investigated. The first one is the determination of an accurate macroscopic strength criterion or plastic yield surface for dry porous materials without fluid phases by

taking into account the effect of porosity. The second one is to study the effects of fluid phases such as fluid pressures, saturation degree, etc. Different kinds of approaches can be adopted to investigate these two aspects, mainly including macroscopic phenomenological models and micro-mechanics based models. The objective of the present paper is to address the first objective by using micro-mechanics based approaches, more precisely, the determination of macroscopic strength criteria of dry porous materials by using nonlinear homogenization techniques.

Around this objective, a series of studies have been performed during several decades. For pressure-independent metal porous materials, the solid phase is generally represented by the von Mises type material. The pioneer's work has been realized by [17]. An analytical strength criterion has been obtained by considering a hollow sphere and by using a limit analysis method. In order to better fit experimental evidences and numerical results, a number of extensions of this criterion have been proposed. For example, by introducing some heuristic modifications of the Gurson's criterion [47, 48], the so-called GTN (Gurson-Tvergaard-Needelman) model has been established and it is now widely used for metal materials. In some recent criteria [25, 27, 5], the effect of pore size has been taken into account. Two populations of voids at different scales have even been considered in other criteria [49, 50]. The effect of void shape has also been studied [14, 15, 22, 26]. Associated with specific voids nucleation and growth criteria, analytical strength criteria have been used for the analysis of ductile failure in metal materials.

As a fundamental difference with metal materials, due to internal friction, porous geo-materials as well as some polymers are generally constituted of a pressure-dependent solid matrix. The strength under compression is significantly larger than that under tension. Therefore, it is needed to develop new criteria to describe the macroscopic strength of this class of porous materials by taking into account the pressure sensitivity of solid matrix. Some heuristic macroscopic criteria have first been formulated [23, 21, 20]. Concerning the use of homogenization techniques to determine the macroscopic strength criteria, due to its simple linear function, the Drucker-Prager criterion is widely adopted to characterize the local strength of solid phase. For instance, some analytical criteria have been obtained by the limit analysis approach [16, 37], by the modified secant method [3, 24]. Some other methods have also been proposed, for example by expending the yield function in powers of porosity [13], and by adopting a stress variational method [8]. By using these analytical criteria as yield functions and introducing suitable hardening laws, different plastic models have been established to describe full stress-strain relations of rocks and concrete materials. Further, by adopting a two-step homogenization procedure, some analytical strength criteria and plastic models have been developed for materials containing pores at a small scale and

rigid inclusions at a large scale [41, 39, 18, 4]. Some authors have also studied double porous materials with small and big pores and pressure-sensitive solid phase [38, 35, 34, 36].

On the other hand, although not investigated in this paper, a series of interesting studies have been performed to investigate the effects of pore fluids on the macroscopic mechanical behavior of rocks and soils, for instance [32, 33, 43, 52, 51, 2]. Those previous studies provide a sound background for the extension of strength criteria for dry porous materials to saturated or partially saturated conditions.

In spite of different existing studies around the determination of macroscopic criteria of dry porous materials by micro-mechanics based approaches, there is a need to make a detailed evaluation of representative existing criteria. Further, the accuracy of most existing criteria is not really satisfactory compared with reference results obtained from direct numerical simulations. Therefore, two main objectives are given to this work. The first one is to make an in-depth evaluation of selected existing analytical criteria by making original theoretical comparisons between them. On the other hand, new numerical results are provided in this study by making direct finite element simulations. These numerical results are used to check the accuracy of the selected criteria. In particular, the estimation of the pure shear strength $\frac{\Sigma_{eq}}{\sigma_0}$ is discussed in depth. Based on the theoretical and numerical evaluations, a new macroscopic strength criterion is determined. The new criterion significantly improves the prediction of the pure shear strength with respect to all the selected criteria. Furthermore, this new criterion is validated by new numerical results for a wide range of porosity and frictional parameter, also for the special case with a pressure-independent matrix.

2. Theoretical evaluation of main macroscopic criteria

In the section, we present a theoretical evaluation of the main exiating representative macroscopic criteria for porous media whose solid phase obeys to the Drucker-Prager (D-P) model. For this purpose, we first recall some common background features for these models.

At the microscale, the matrix is described by the following D-P criterion:

$$\Phi(\boldsymbol{\sigma}) = \sigma_{eq} + 3\alpha\sigma_m - \sigma_0 \leq 0 \tag{1}$$

in which $\sigma_m = tr\boldsymbol{\sigma}/3$ and $\sigma_{eq} = \sqrt{\frac{3}{2}\boldsymbol{\sigma}' : \boldsymbol{\sigma}'}$, $\boldsymbol{\sigma}'$ is the deviatoric part of the local stress $\boldsymbol{\sigma}$. α and σ_0 are material parameters, the frictional coefficient and the strength in the case of purely shear loading, respectively.

According to [31], the support function $\pi(\boldsymbol{d})$ of the D-P matrix described by equation

(1) at the microscopic scale can be calculated as follows:

$$\pi(\boldsymbol{d}) = \begin{cases} \dfrac{\sigma_0}{\alpha} d_m & \text{if} \quad d_m \geq \alpha d_{eq} \\ +\infty & \text{if} \quad d_m < \alpha d_{eq} \end{cases} \tag{2}$$

where $\boldsymbol{d}$ is the strain rate, $d_m = tr(\boldsymbol{d})/3$ and $d_{eq} = \sqrt{\frac{2}{3}\boldsymbol{d}' : \boldsymbol{d}'}$.

By considering either the normality rule or the non-associated one for the solid matrix, we shall obtain two different categories of macroscopic strength criteria, that are respectively discussed in the following sub-sections.

2.1. Porous materials with associated flow solid matrix

In the first case of an associated flow rule in matrix at the microscale, we consider here two types of void shape, respectively spherical void and spheroidal void.

2.1.1. Porous materials with spherical void

- Heuristic criterion proposed by [23] The von Mises criterion is modified by adding a main stress related term: $\Phi(\boldsymbol{\sigma}) = \sigma_{eq}^2 - (\sigma_0 - 3\alpha\sigma_m)^2 = 0$, which is the particular case of Drucker-Prager criterion (1). Based on the expression of the Gurson's criterion, a heuristic extension of the Gurson's criterion is there proposed:

$$\frac{\Sigma_{eq}^2}{\sigma_0^2} + 3\alpha\frac{\Sigma_m}{\sigma_0}\left(2 - 3\alpha\frac{\Sigma_m}{\sigma_0}\right) + 2f\cosh\left(\frac{3\Sigma_m}{2\sigma_0}\right) - 1 - f^2 = 0 \tag{3}$$

- Criterion proposed by [21] and [20] based on some special cases

  In [21], the hydrostatic tensile strength of the studied porous material with Drucker-Prager matrix has been derived: $\frac{\Sigma_m}{\sigma_0} = \frac{1 - f^{\frac{2\alpha}{2\alpha+1}}}{3\alpha}$. Taking into account some special conditions, $f \to 0$ and $\alpha \to 0$, a macroscopic criterion was given in [21]:

$$\left(\frac{\Sigma_{eq} + 3\alpha\Sigma_m}{\sigma_0}\right)^2 + 2f\cosh\left[\frac{1+\alpha}{2\alpha}\ln\left(1 - 3\alpha\frac{\Sigma_m}{\sigma_0}\right)\right] - 1 - f^2 = 0 \tag{4}$$

  This criterion was good for the positive mean stress domain but not suitable for the compressive domain. Therefore, [1] has proposed the following function for the compressive mean stress domain:

$$\left(\frac{\Sigma_{eq} + 3\alpha\Sigma_m}{\sigma_0}\right)^2 + 2f - 1 - f^2 = 0 \tag{5}$$

This criterion (5) does not provide the exact hydrostatic compression strength. An amelioration was done in [20] by calculating the exact hydrostatic tensile and compression strengths as follows:

$$\frac{\Sigma_m}{\sigma_0} = \frac{1 - f^{2\alpha/(2\alpha+sign(\Sigma_m))}}{3\alpha} \tag{6}$$

Then, another improved macroscopic criterion was established in [21]:

$$\left(\frac{\frac{\Sigma_{eq}}{\sigma_0}}{1-3\alpha\frac{\Sigma_m}{\sigma_0}}\right)^2 + 2f\cosh\left[\frac{1+sign(\Sigma_m)2\alpha}{2\alpha}\ln\left(1-3\alpha\frac{\Sigma_m}{\sigma_0}\right)\right] - 1 - f^2 = 0 \tag{7}$$

- Criterion derived in [3] with the modified secant method

  By adopting the modified secant method, [3] has obtained an explicit expression of macroscopic strength function for the studied porous materials. The original criterion is rewritten here by using the same variables as in other criteria:

$$\left(1+\frac{2}{3}f\right)\frac{\Sigma_{eq}^2}{\sigma_0^2} + \left(\frac{9}{4}f - 9\alpha^2\right)\frac{\Sigma_m^2}{\sigma_0^2} + 6\alpha(1-f)\frac{\Sigma_m}{\sigma_0} - (1-f)^2 = 0 \tag{8}$$

- Criterion established by limit analysis approach [16]

  By choosing a hollow sphere as the representative elementary volume with a uniform strain rate boundary condition, the following implicit macroscopic function $\Phi(\Sigma_{eq}(\varpi), \Sigma_m(\varpi))$ is first derived by [16] in the framework of limit analysis:

$$\frac{\Sigma_{eq}}{\sigma_0} = \frac{f^\gamma - f}{f^\gamma - f + \alpha\partial F/\partial C_0}\frac{\partial F}{\partial D_e} \qquad 3\frac{\Sigma_m}{\sigma_0} = \frac{1-f}{f^\gamma - f + \alpha\partial F/\partial C_0}\frac{\partial F}{\partial C_0} \tag{9}$$

  where $\varpi = \frac{2C_0}{sD_e}$ ranges from $-\infty$ to ∞, $s = 1 \pm 2\alpha$, $\gamma = 1 - s^{-1}$. The parameters $\frac{\partial F}{\partial D_e}$ and $\frac{\partial F}{\partial C_0}$ are given as functions of Gauss hypergeometric function (${}_2F_1(a,b;c;z)$):

$$\begin{cases} \frac{\partial F}{\partial C_0} = \frac{\varpi}{s/2-1}\left[{}_2F_1(\frac{1}{2}, 1-\frac{s}{2}; 2-\frac{s}{2}; -\varpi^2) - f^{1-2/s}\ {}_2F_1(\frac{1}{2}, 1-\frac{s}{2}; 2-\frac{s}{2}; -\frac{\varpi^2}{f^{2/s}})\right] \\ \frac{\partial F}{\partial D_e} = {}_2F_1(\frac{1}{2}, -\frac{s}{2}; 1-\frac{s}{2}; -\varpi^2) - f\ {}_2F_1(\frac{1}{2}, -\frac{s}{2}; 1-\frac{s}{2}; -\frac{\varpi^2}{f^{2/s}}) \end{cases} \tag{10}$$

  This model is called "Upper bound model" (UBM) by the authors. For the purpose to establish an explicit expression of the overall yield function, the authors have considered some particular cases. An approximate function has been derived in [16]:

$$\left(\frac{\frac{\Sigma_{eq}}{\sigma_0}}{\Theta}\right)^2 + 2f\cosh\left[\frac{sign(\Sigma_m)+2\alpha}{2\alpha}\ln\left(1-3\alpha\frac{\Sigma_m}{\sigma_0}\right)\right] - 1 - f^2 = 0 \tag{11}$$

in which two expressions of Θ are provided in [16]: $\Theta_1 = 1 - \frac{3\alpha}{(1-f)^{1-s/2}}\frac{\Sigma_m}{\sigma_0}$ and $\Theta_2 = 1 - \frac{3\alpha}{1+\gamma\ln(1+sf)}\frac{\Sigma_m}{\sigma_0}$.

- Criterion obtained by expending yield criterion in powers of porosity f [13]

  Another approach is used in [13]. The derivation is based on expending the yield criterion in powers of porosity f. The local yield criterion of the matrix is found when the zero order is given. Taking the second order power expansion, a macroscopic criterion is obtained:

$$\frac{\Sigma_{eq}^2}{\sigma_0^2} - (1 - 3\alpha\frac{\Sigma_m}{\sigma_0})^2 + 2f(1 - 3\alpha\frac{\Sigma_m}{\sigma_0})\cosh\left[\frac{1}{2\alpha}\ln\left(1 - 3\alpha\frac{\Sigma_m}{\sigma_0}\right)\right] - f^2 = 0 \tag{12}$$

- Criterion given by [8] based on a stress variational method

  In the study [8], the macroscopic criterion is derived by using a stress-based approach called stress variational method. With a stress field which is not totally statically admissible, one gets the following effective yield function:

$$\frac{\Sigma_{eq}}{\sigma_0(1-f)}\left[{}_2F_1(-\tfrac{1}{2},-\tfrac{1}{2w};1-\tfrac{1}{2w},-\varrho^2) - f\ {}_2F_1(-\tfrac{1}{2},-\tfrac{1}{2w};1-\tfrac{1}{2w},-\tfrac{\varrho^2}{f^{2w}})\right] + 3\alpha\frac{\Sigma_m}{\sigma_0} - (1-f) \le 0 \tag{13}$$

  in which $\varrho = \frac{3w(1-f)}{2(1-f^{-w})}\frac{\Sigma_m}{\Sigma_{eq}}$, $w = 2\alpha/(2\alpha \pm 1)$.

2.1.2. Porous materials with spheroidal void [37]

The above existing yield criteria are for porous material with a D-P matrix and spherical pore. Some contributions have been done to study the influence of pore shape on the plastic yield surface. The spheroidal pores (oblate or prolate) have been considered. Considering a representative volume elements made up of a spheroidal domain containing a spheroidal confocal void and a suitable velocity field, an approximate macroscopic criterion is established in the following form by the limit analysis approach:

$$\mathfrak{R}^2\left[\frac{\Sigma_{eq}^2}{\sigma_0^2} + \frac{\left(\tau(3\alpha_2-1)\frac{\Sigma_{eq}^2}{\sigma_0^2} + \frac{\Sigma_s}{\Theta} + \frac{\Sigma_q}{\sigma_0}\right)^2 + (\zeta-1)\frac{\Sigma_q^2}{\sigma_0^2}}{1-\zeta}\right] + 2(1+g)(f+g)\cosh\left(\frac{\Gamma}{p}\right) - (1+g)^2 - (f+g)^2 = 0 \tag{14}$$

where the parameters used in criterion (14) are given in Appendix B.

In the case of spherical void, the function (14) can be simplified as:

$$\frac{\frac{\Sigma_{eq}^2}{\sigma_0^2}}{\left[1-\frac{3\alpha}{(1-f)}\frac{\Sigma_m}{\sigma_0}\right]^2}+2f\cosh\left(\frac{2\alpha+sgn(\Sigma_m)}{2\alpha}\ln(1-3\alpha\frac{\Sigma_m}{\sigma_0})\right)-1-f^2=0 \tag{15}$$

2.2. Porous media having a non-associated D-P matrix

On the other hand, some researchers have studied the influence of non-associated flow rule of the matrix on the overall mechanical behavior, such as macroscopic yield function and plastic potential.

- Macroscopic criterion and plastic potential proposed by [24]

  By adopting a non-associated flow rule for the D-P type matrix, the work in [3] has been extended in [24] with a local plastic potential:

  $$\phi(\boldsymbol{\sigma})=\sigma_{eq}+3\beta\sigma_m \tag{16}$$

  where β denotes the plastic dilatancy coefficient with $0\leq\beta\leq\alpha<\frac{1}{2}$.

  However, the macroscopic yield function with a non-associated D-P matrix obtained in [24] remains identical to the one (8) given by [3] with an associated D-P matrix. This yield function is independent of the dilatancy coefficient β. However, it is possible to determine a macroscopic plastic potential which depends on β:

  $$G=\left(1+\frac{2}{3}f\right)\frac{\Sigma_{eq}^2}{\sigma_0^2}+\left(\frac{9}{4}f-9\alpha\beta\right)\frac{\Sigma_m^2}{\sigma_0^2}+6\beta(1-f)\frac{\Sigma_m}{\sigma_0} \tag{17}$$

- Macroscopic criterion proposed by [9]

  A hollow sphere having a non-associated D-P matrix has been investigated in [9]. The bi-potential theory proposed by [12, 10, 11, 19] has been adopted to extend the limit analysis method. Following the minimization procedure and solving the saddle point problem, a macroscopic strength criterion is derived:

  $$\begin{cases}\dfrac{\Sigma_{eq}}{\sigma_0}=\dfrac{f^{\tilde{\gamma}}-f\left[\frac{\beta}{\alpha}\Pi_{D_e}+\left(1-\frac{\beta}{\alpha}\right)\hat{\Pi}_{D_e}\right]+\left(1-\frac{\beta}{\alpha}\right)\beta\left(\Pi_{C_0}\hat{\Pi}_{D_e}-\Pi_{D_e}\hat{\Pi}_{C_0}\right)}{f^{\tilde{\gamma}}-f+\beta\Pi_{C_0}}\\ 3\dfrac{\Sigma_m}{\sigma_0}=(1-f)\dfrac{\frac{\beta}{\alpha}\Pi_{C_0}+\left(1-\frac{\beta}{\alpha}\right)\hat{\Pi}_{D_e}}{f^{\tilde{\gamma}}-f+\beta\Pi_{C_0}}\end{cases} \tag{18}$$

  The parameters Π_{C_0}, Π_{D_e}, $\hat{\Pi}_{C_0}$, $\hat{\Pi}_{D_e}$, $\mathcal{P}(\tau)$ and $\tilde{\gamma}$ are given in Appendix C.

  For a general loading, the yield strength in the non associated case is slight lower than the one in associated case in the compressive loading. There is no great different in the tensile loading.

2.3. Recapitulation of the existing macroscopic criteria

For the purpose of clarity, the selected macroscopic yield functions for porous media having a D-P matrix are recapitulated in Appendix A with the corresponding derivation method used. When the pores are spherical, the exact solutions of strength for hydrostatic tension and compression can be retrieved by the criteria (7), (9), (11), (12), (13), (15) and (18). Concerning the pure deviatoric loading ($\Sigma_m = 0$), the value of $\frac{\Sigma_{eq}}{\sigma_0}$ given by (8) with the modified secant method is $\frac{1-f}{\sqrt{1+\frac{2}{3}f}}$, which is different from the value of $(1-f)$ obtained in all other criteria.

3. Evaluations and comparisons of yield criteria by new FEM numerical results

Based on the summary of the main existing macroscopic yield criteria, it is therefore interesting and important to evaluate their accuracies. To this end, a series of new numerical results are carried out in this study by FEM method. This numerical method will be firstly evaluated by comparing with numerical limit analysis results.

3.1. Verification of finite element simulation

The representative volume element of porous material is here represented by a hollow sphere. Due to its axi-symmetric property, only a quarter of the hollow sphere is considered and it is meshed with 900 quadratic quadrilateral elements of type CAX8 and with 2821 nodes in Abaqus software, as illustrated in Figure 1(a) for the case $f = 0.1$. The solid matrix obeys the Drucker-Prager plastic criterion (1). With the assumption of small strains, the displacement velocity field is prescribed on the exterior boundary of the hollow sphere. A user subroutine MPC (Multi-Points Constraints) is used in this study for the loading condition with a constant macroscopic stress triaxiality $T = \Sigma_m/\Sigma_{eq}$, which is realized by calculating the constant stress ratio Σ_ρ/Σ_z as the one done in [7, 16].

In Figures 1(b) and 1(c), we compare the finite element results with the numerical bounds proposed in [29], by employing the limit analysis and a second order conic programming. The porosity selected is $f = 0.1$, the frictional parameter are $\alpha = 0.1/3,\ 0.83205/3$, respectively. The red points are the upper bounds and the green ones are the lower bounds. The asterisks present the FEM results. The black solid ones are the hydrostatic values given by (6). In these figures, the red points are very close to the green ones which indicates that they are approach to the exact solution. On the other hand, the FEM results are also very close to the numerical bounds and have a good accuracy. Figure 1(d) presents the case of a spheroidal void (oblate $a_1/b_1 = 1/2$) for porosity $f = 0.1$ with different friction angles. Again, the FEM solutions are well framed by the lower and upper bounds. According to the comparisons

for these two different cases, the finite element simulations are well validated and these numerical solutions will be adopted to evaluate the above selected analytical yield criterion.

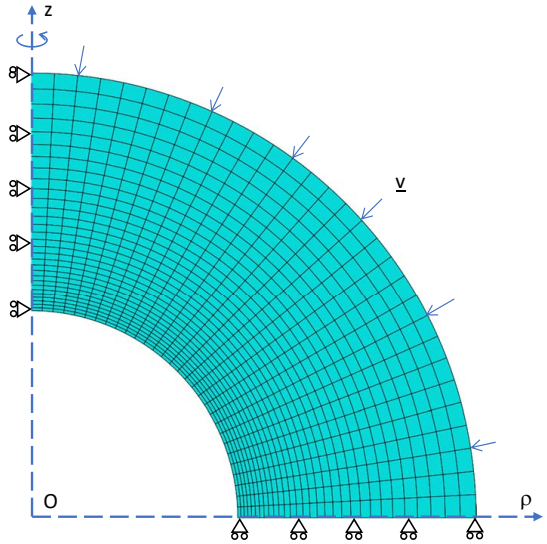

(a) Mesh, $f = 0.1$, spherical pore

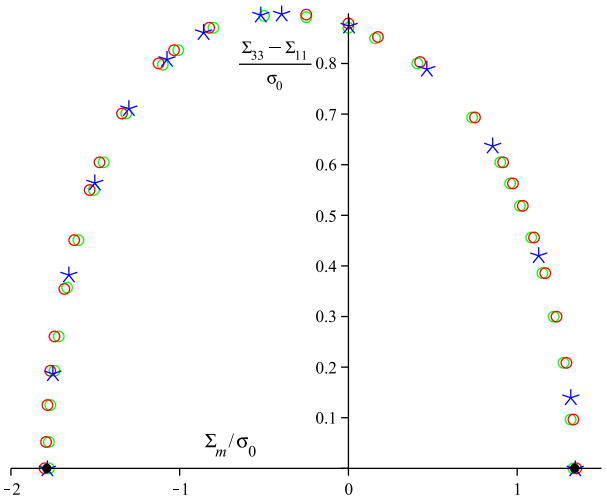

(b) $\alpha = 0.1/3$, $f = 0.1$

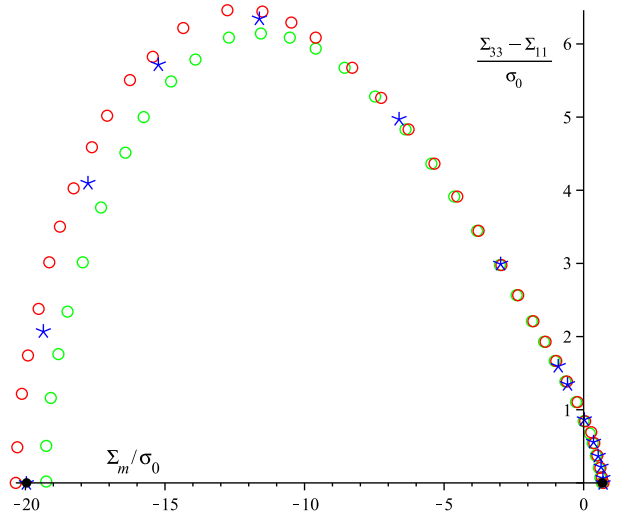

(c) $\alpha = 0.83205/3$, $f = 0.1$

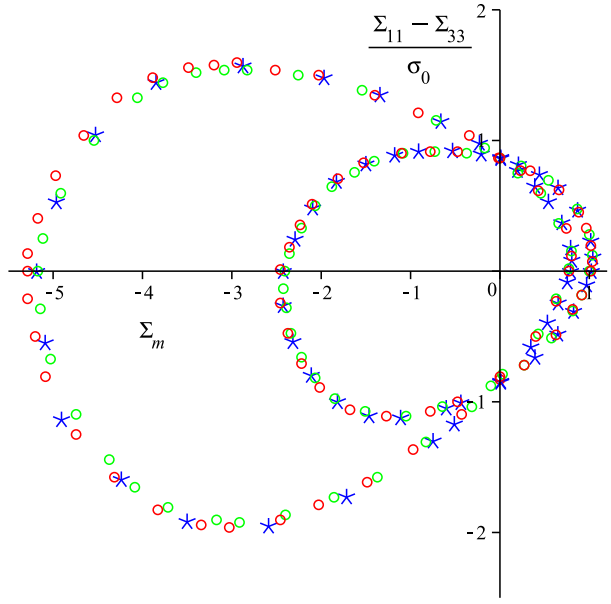

(d) frictional angle: $16.7°, 30.2°$, $f = 0.1$

Figure 1: Validations of the FEM results (asterisk) by the upper (red circle) and lower (green circle) bounds proposed by [29] (spherical pore, -b and -c) and by [28] (spheroidal pore -d: $a_1/b_1 = 1/2$).

3.2. Assessment of analytical criteria by new numerical solutions

The macroscopic criteria are now assessed and evaluated through the comparison with FEM results. For this purpose, we consider a wide range of porosity f = 0.04, 0.1, 0.15, 0.2, 0.3, 0.4 and frictional parameter α = 0, 0.05, 0.1, 0.15, 0.2, 0.25, 0.3 (the corresponding friction angles are ϕ = 0, 8.53°, 16.70°, 24.23°, 30.96°, 36.87°, 41.99°). The cases of f = 0.04 and 0.4 are illustrated in Figures 2 and 3, another porosities are shown in Appendix D. In these in Figures, FEM results are presented by black points. The solid green circles denote the hydrostatic results. Different lines are used to show the yield surfaces predicted by the above analytical criteria: (7)-black line, (8)-sky blue line, (9)-red solid line, (11) with Θ_1-red dash dot line, (11) with Θ_2-red dash line, (12)-green line, (15)-blue line.

One can see that all the criteria except (8) are very close to each other when the porosity f and frictional parameter α are small. The exact solution when $\Sigma_{eq} = 0$ cannot be retrieved by (8). However, the value $\frac{\Sigma_{eq}}{\sigma_0}$ predicted in (8), $\frac{1-f}{\sqrt{1+2f/3}}$, is closer to the FEM results than that, $(1-f)$, given by the other criteria when the porosity f is small. Nevertheless, these two analytical values of $\frac{\Sigma_{eq}}{\sigma_0}$ are all very different from the FEM results when $f > 0.15$. This point about the value of $\frac{\Sigma_{eq}}{\sigma_0}$ for $\Sigma_m = 0$ will be especially studied in depth in the following section.

The yield surface (black line) predicted by the criterion (7) proposed in [20] coincides well with the one (green line) (12) given in [13] when $f < 0.2$. In the case of $f > 0.2$, there is a good agreement between (12) (green line) and (9) (red solid line).

In the tension zone, the analytical criteria have a good prediction comparing with FEM results. However, the prediction of the criterion (15)(blue line) is closer to FEM solutions than other ones. In the compressive zone, the strength surfaces predicted by (15) and (11) with Θ_1 are always outside of the FEM results.

It is worth to mention that the criterion (9) (red solid line) underestimates the strength when the frictional parameter α is big, for example, α = 0.2, 0.25, 0.3. This observation also confirms the remarks made in some previous studies [45, 30, 44, 29]. The so-called "upper bound model" (parametric criterion (9)) is not a rigorous upper bound, however, it is a good approximation.

The relative errors [1] between the FEM numerical results and the predictions given by

[1] The relative error is calculated by the following formula:

$$\text{Relative error } (X) = \left|\frac{X \text{ predicted by criterion} - X \text{ given by Abaqus}}{X \text{ given by Abaqus}}\right| \cdot 100\%$$

Two stress values (Σ_m and Σ_{eq}) are considered in each point, respectively by putting $X = \Sigma_m$ for the relative error of macroscopic mean stress and $X = \Sigma_{eq}$ for the one of macroscopic equivalent stress. The smaller one

these macroscopic criteria are illustrated in Figure 4 for different cases with $f = 0.2$, $\alpha = 0.15$, $f = 0.2$, $\alpha = 0.3$ and $f = 0.4$, $\alpha = 0.15$, as functions of macroscopic stress triaxiality $T = \Sigma_m/\Sigma_{eq}$. In a general way, according to the comparisons between analytical predictions and FEM results, it seems that the criterion (11) with Θ_2 and the one (12) provide the most accuracy estimation of material strength.

of both is then chosen to plot the relative error maps.

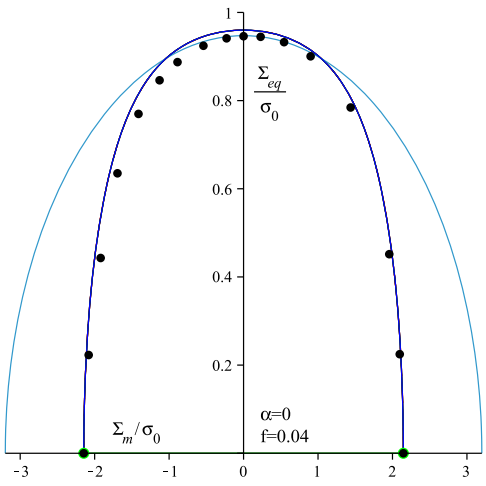

(a) $f = 0.04$, $\alpha = 0$

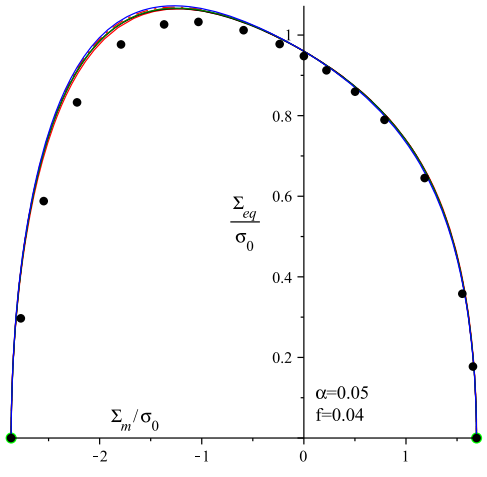

(b) $f = 0.04$, $\alpha = 0.05$

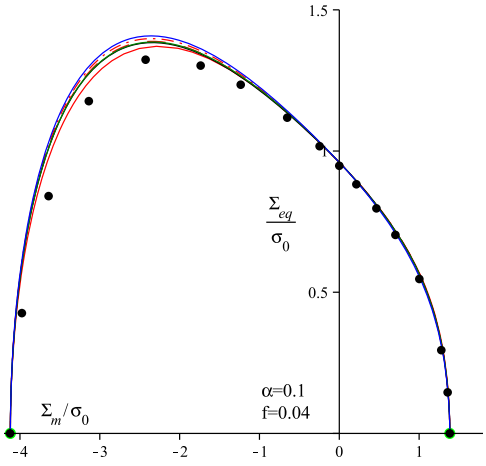

(c) $f = 0.04$, $\alpha = 0.1$

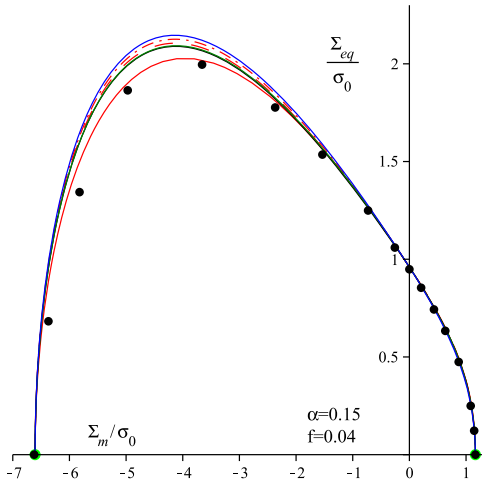

(d) $f = 0.04$, $\alpha = 0.15$

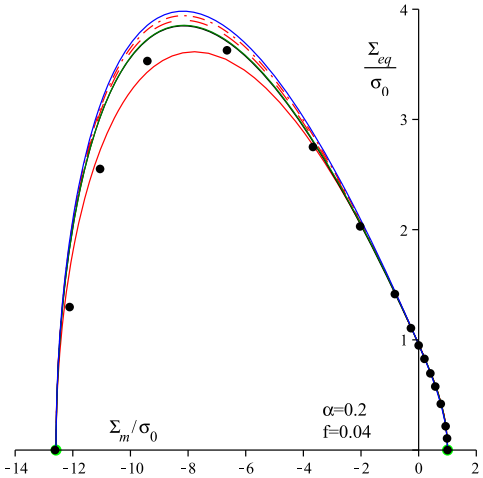

(e) $f = 0.04$, $\alpha = 0.2$

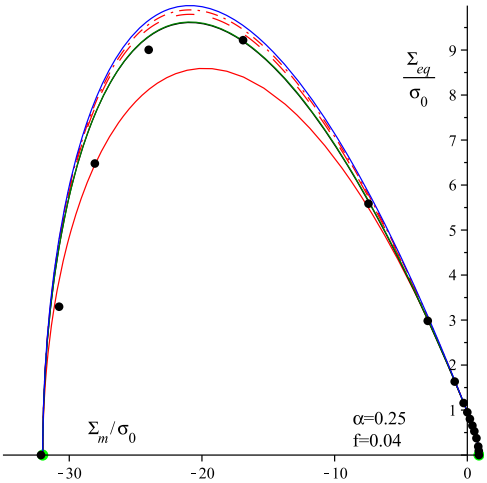

(f) $f = 0.04$, $\alpha = 0.25$

Figure 2: Comparisons of yield surfaces predicted by criteria (7)-black line, (8)-skyblue line, (9)-red solid line, (11) with Θ_1- red dashdot line, (11) with Θ_2-red dash line, (12)-green line, (15)-blue line and FEM solutions with different α, $f = 0.04$.

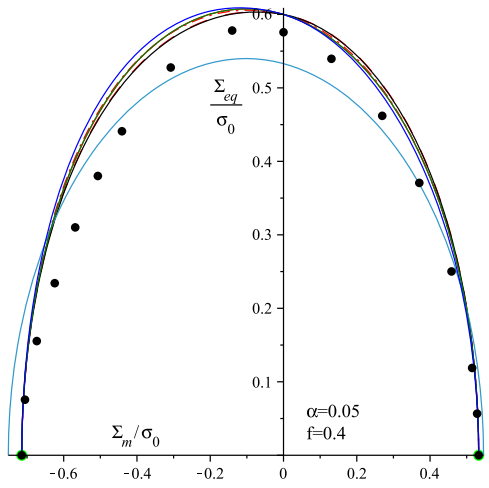

(a) $f = 0.4$, $\alpha = 0.05$

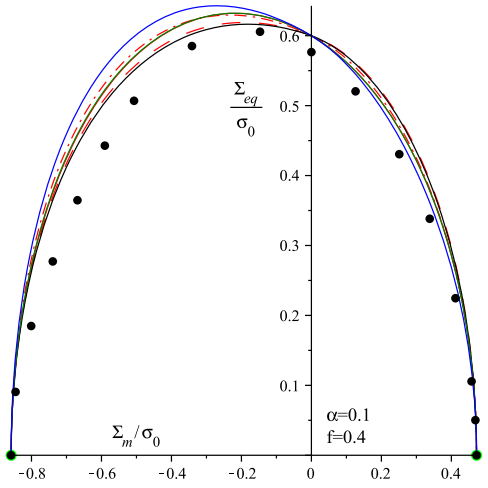

(b) $f = 0.4$, $\alpha = 0.1$

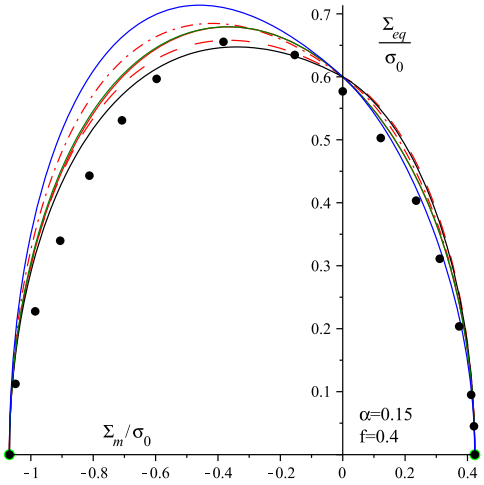

(c) $f = 0.4$, $\alpha = 0.15$

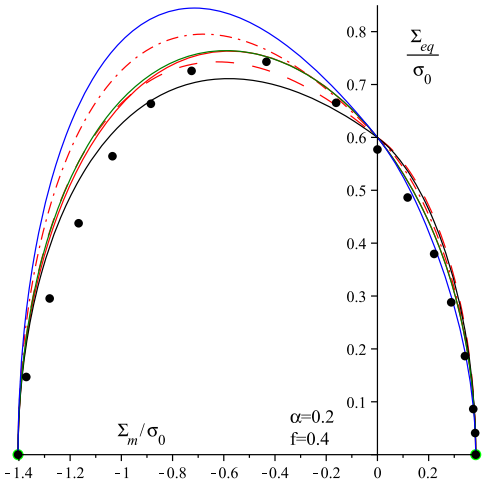

(d) $f = 0.4$, $\alpha = 0.2$

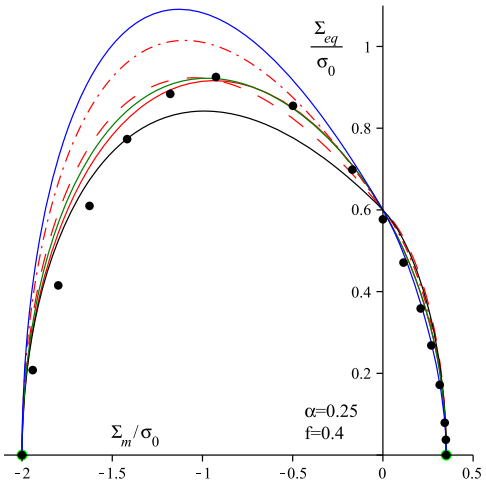

(e) $f = 0.4$, $\alpha = 0.25$

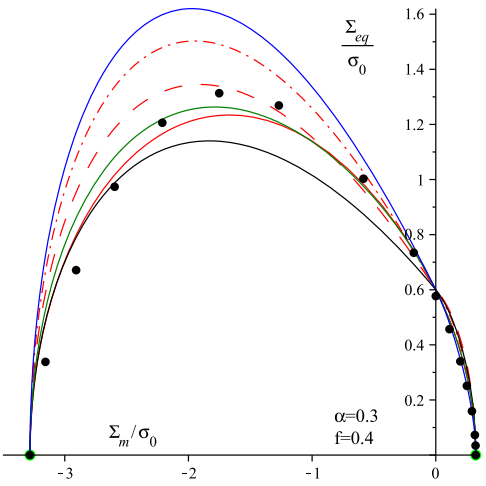

(f) $f = 0.4$, $\alpha = 0.3$

Figure 3: Comparisons of yield surfaces predicted by criteria (7)-black line, (8)-skyblue line, (9)-red solid line, (11) with Θ_1- red dashdot line, (11) with Θ_2-red dash line, (12)-green line, (15)-blue line and FEM solutions with different α, $f = 0.4$.

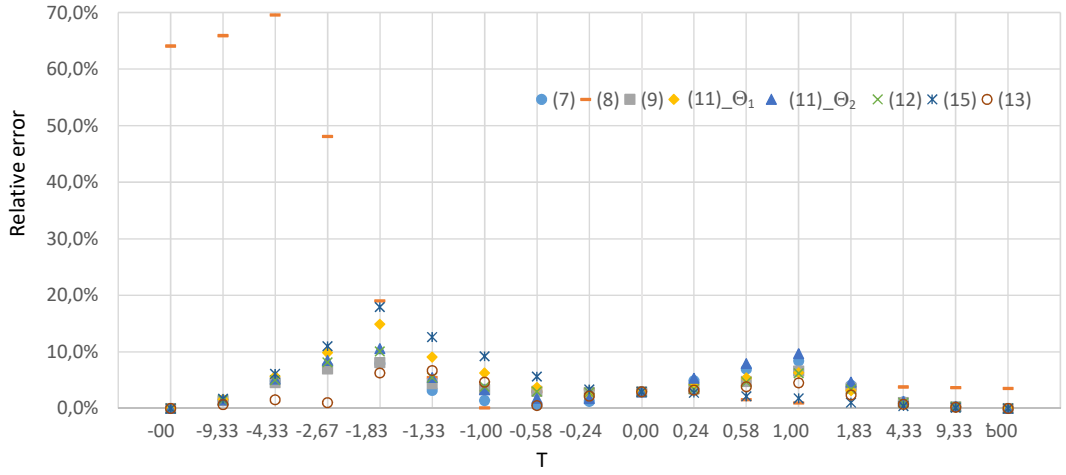

(a) $f = 0.2$, $\alpha = 0.15$

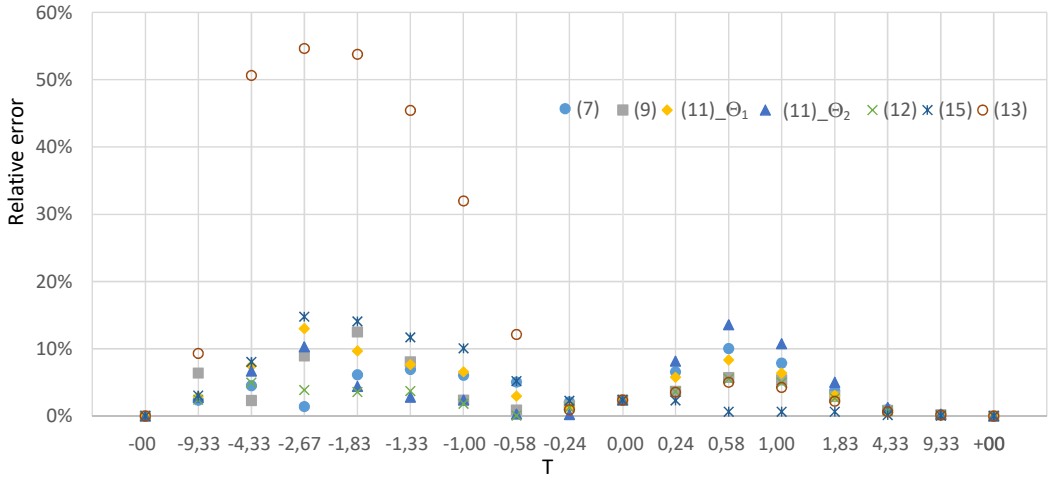

(b) $f = 0.2$, $\alpha = 0.3$

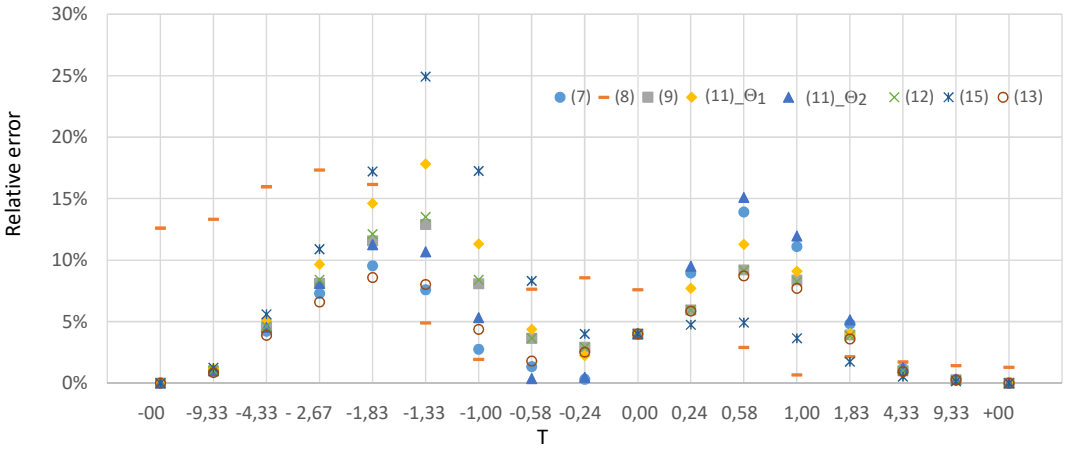

(c) $f = 0.4$, $\alpha = 0.15$

Figure 4: Relative errors between the numerical results and predictions of yield criteria with different porosity and frictional parameter.

4. Numerical investigation of the strength prediction in pure shear loading

As indicated in the previous section, two different values of shear strength $\frac{\Sigma_{eq}}{\sigma_0}$ are provided by the selected criteria when $\frac{\Sigma_m}{\sigma_0} = 0$: $\frac{1-f}{\sqrt{1+\frac{2}{3}f}}$ by [3, 24] and $(1-f)$ by the other ones. Both values depend on the porosity f. However, the influence of the frictional parameter α on the shear strength $\frac{\Sigma_{eq}}{\sigma_0}$ when $\frac{\Sigma_m}{\sigma_0} = 0$ is so far not explicitly studied. In this study, this issue is investigated by direct FEM simulations. We consider then different porosity and frictional parameter: $f = 0.04, 0.1, 0.2, 0.3, 0.4, 0.6, 0.8$ and $\alpha = 0, 0.1, 0.2, 0.3, 0.4, 0.49$.

As shown in Figure 5, the porosity affects importantly the pure shear strength. The increase of porosity leads to a quick decrease of $\frac{\Sigma_z - \Sigma_\rho}{\sigma_0}$. Due to the influence of third stress invariant, the strength of the studied parous material is not symmetric with respect to $\frac{\Sigma_z - \Sigma_\rho}{\sigma_0}$. When $\Sigma_z - \Sigma_\rho > 0$, the frictional coefficient α has a slight influence. However, this influence can be neglected for $\Sigma_z - \Sigma_\rho < 0$. As for all the analytical criteria selected here, the quantity $\frac{\Sigma_{eq}}{\sigma_0} = \frac{|\Sigma_z - \Sigma_\rho|}{\sigma_0}$ is independent of α. Therefore, we present here the FEM results for $\Sigma_z - \Sigma_\rho < 0$ only.

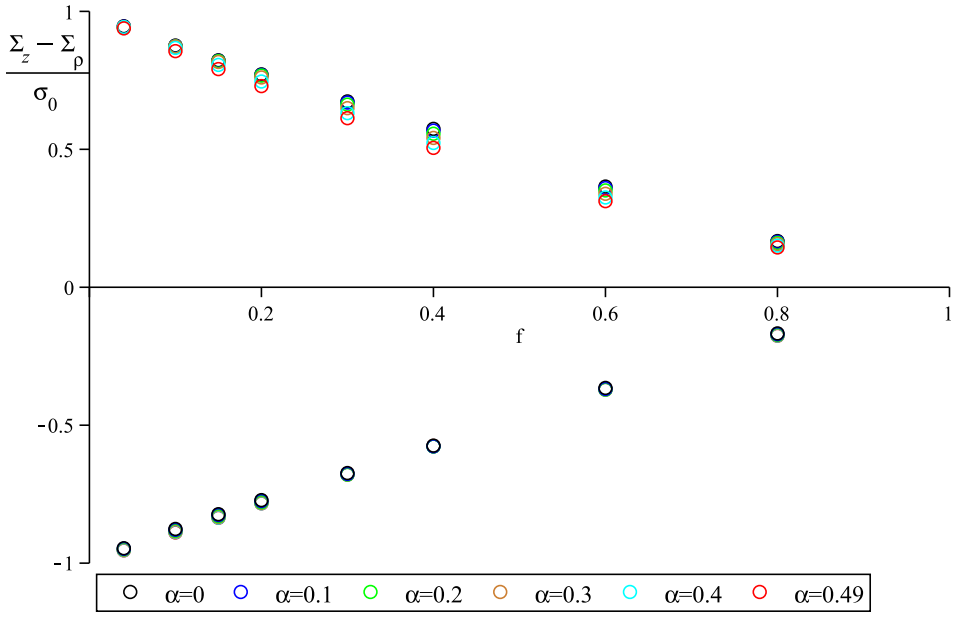

Figure 5: FEM solutions of $\frac{\Sigma_z - \Sigma_\rho}{\sigma_0}$ for pure deviatoric loading ($\frac{\Sigma_m}{\sigma_0} = 0$) with different f and α.

We compare now the numerical values of pure shear strength $\frac{\Sigma_{eq}}{\sigma_0}$ with two theoretical predictions: $(1-f)$ and $\frac{1-f}{\sqrt{1+\frac{2}{3}f}}$. The comparisons are presented on Figure 6. One can see that the value $(1-f)$ is always over the FEM results and represents a sort of upper bound.

For small or very big values of porosity f, the value $\frac{1-f}{\sqrt{1+\frac{2}{3}f}}$ coincides well with the numerical results, but it is lower for intermediate values of porosity.

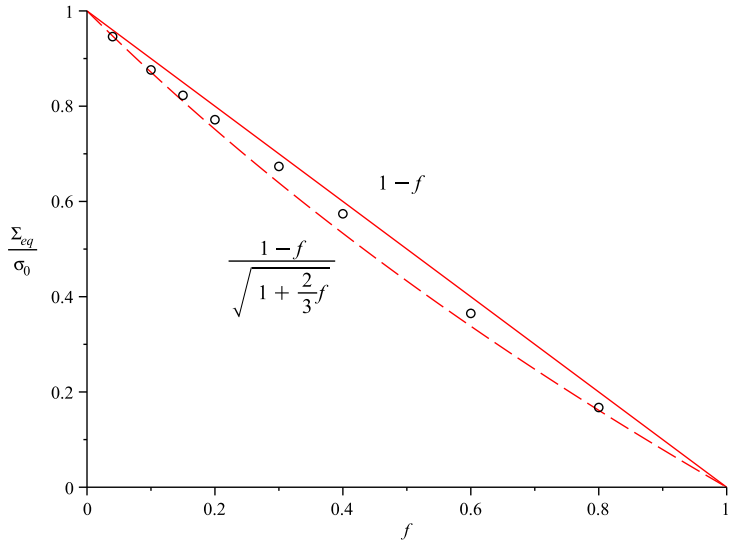

Figure 6: Comparisons between $\frac{\Sigma_{eq}}{\sigma_0}$ given by existing criteria and the one of FEM for pure deviatoric loading ($\frac{\Sigma_m}{\sigma_0} = 0$): Dashed line: $\frac{1-f}{\sqrt{1+2f/3}}$ given by [3, 24]; Solid line : $(1-f)$ given by other criteria.

5. Theoretical improvement of the strength prediction in pure shear loading

Based on the above comparisons, some new improvements will be provided firstly to ameliorate the performance in pure shear loading for porous media having a D-P matrix. For this purpose, the stress variational homogenization method will be used with a statically admissible stress field which will be constructed in this work.

5.1. Brief recall of stress variational approach

The stress variational approach was proposed in [6, 40, 42], and its main lines are here briefly recalled. In this study, the matrix is pressure-sensitive and obeys to the local yield critetion (1), a statically admissible stress field will be constructed for this material to derive a macroscopic yield criterion with the effect of porosity.

According to the normality law, the strain rate tensor $\mathbf{d}$ is given as:

$$\mathbf{d} = \dot{\lambda}\frac{\partial \Phi}{\partial \boldsymbol{\sigma}}(\boldsymbol{\sigma}) \tag{19}$$

in which $\dot{\lambda}$ is the plastic multiplier.

Then the Hill's inequality can be expressed as:

$$\forall \boldsymbol{\sigma}' \in P, \qquad (\boldsymbol{\sigma}' - \boldsymbol{\sigma}) : \mathbf{d} \leq 0 \ , \tag{20}$$

where P is the plastic bound defined by the local yield criterion (1).

According to the local stress and strain ($\boldsymbol{\sigma}$ and $\mathbf{d}$), the macroscopic ones ($\boldsymbol{\Sigma}$ and $\mathbf{D}$) can be computed by the homogenisation approach:

$$\boldsymbol{\Sigma} = \frac{1}{|\ \Omega\ |} \int_{\Omega} \boldsymbol{\sigma}\ dV \ , \qquad \mathbf{D} = \frac{1}{|\ \Omega\ |} \int_{\Omega} \mathbf{d}\ dV \ . \tag{21}$$

Based on the conception on convex analysis, a semi-continuous function $\varphi(\boldsymbol{\sigma})$ is introduced as follows: which is 0 if $\boldsymbol{\sigma} \in P$ and $+\infty$ otherwise.

Then, the condition (20) can be rewritten as: $\mathbf{d} \in \partial\varphi(\boldsymbol{\sigma})$.

According to the Hill's variational principle, the true stress field minimizes the following functional among all the statically admissible stress fields g_a:

$$\int_{\Omega_M} \varphi(\boldsymbol{\sigma})\ dV - \int_{S_u} (\boldsymbol{\sigma}.\underline{n}).\underline{v}\ dS \tag{22}$$

$$g_a = \{\boldsymbol{\sigma} : \quad div\ \boldsymbol{\sigma} = 0, \quad x \in \Omega; \quad \boldsymbol{\sigma} \cdot \underline{n} = \underline{0}, \quad x \in \partial\omega; \quad \boldsymbol{\sigma} = \mathbf{0}, \quad x \in \omega\} \tag{23}$$

in which $\underline{n}$ is the unit outward normal vector, $\underline{v}$ is the imposed velocity on the boundary S_u of Ω_M. For the studied homogenization problem of a hollow sphere with a boundary condition $\underline{v}(\underline{x}) = \boldsymbol{D}.\underline{x}$, the set of kinematically admissible velocity fields classically reads:

$$\mathcal{K}_a = \{\underline{v} \quad s.t. \quad \underline{v}(\underline{x}) = \mathbf{D} \cdot \underline{x} \quad on \quad \partial\Omega\} \tag{24}$$

Then one gets the following average functional:

$$\min_{\boldsymbol{\sigma} \in g_a} \left(\frac{1}{|\ \Omega\ |} \int_{\Omega_M} \varphi(\boldsymbol{\sigma})\ dV - \mathbf{D} : \boldsymbol{\Sigma} \right) \tag{25}$$

When the stress $\boldsymbol{\sigma}$ is licit, the functional $\varphi(\boldsymbol{\sigma})$ is vanishes. Then, the following minimization problem can be derived from (25) for the studied materials with condition $\Phi(\boldsymbol{\sigma}) = 0$:

$$\min_{\boldsymbol{\sigma} \in g_l} (-\mathbf{D} : \boldsymbol{\Sigma}) \tag{26}$$

where $g_l = \{\boldsymbol{\sigma} \in g_a : \ \Phi(\boldsymbol{\sigma}) \leq 0, \ x \in \Omega_M\}$; g_a is the group of statically admissible which is given in (23).

With the help of the Lagrangian method and the approximation of the condition $\Phi(\boldsymbol{\sigma}) = 0$ by its average value, the above minimization problem can be rewritten as:

$$\max_{\dot{\Upsilon}\geq 0} \min_{\boldsymbol{\sigma}\in g_a} \left(\mathcal{L}(\boldsymbol{\sigma}, \dot{\Lambda}) = \frac{1}{|\,\Omega\,|} \int_{\Omega_M} \dot{\Lambda}\Phi(\boldsymbol{\sigma})\, dV - \mathbf{D} : \boldsymbol{\Sigma} \right) \tag{27}$$

in which $\dot{\Lambda}$ is the Lagrange's multiplier.

By adopting the same value of $\dot{\Lambda}$ in the matrix, the searched overall yield criterion can be calculated as follows:

$$F(\boldsymbol{\Sigma}) = \frac{1}{|\,\Omega\,|} \int_{\Omega_M} \Phi(\boldsymbol{\sigma})\, dV = 0 \tag{28}$$

5.2. Construction of a strict statically admissible field for a D-P type matrix

Based on the general expression of the macroscopic yield criterion (28), the following important step is the construction of a strict statically admissible field $\boldsymbol{\sigma}$ as a function of macroscopic stress. According to [40], a suitable trial stress field could be established and given with three parts: $\boldsymbol{\sigma} = \boldsymbol{\sigma}_1 + \boldsymbol{\sigma}_2 + \boldsymbol{\sigma}_3$, which improves the one used in [8] to derive the criterion (13).

- The exact solution in hydrostatic loading $\boldsymbol{\sigma}_1$

$$\boldsymbol{\sigma}_1 = \frac{A_1}{3\alpha} \left[\left(1 - \left(\frac{a}{r} \right)^{3w} \right) \mathbf{1} + \frac{3}{2} w \left(\frac{a}{r} \right)^{3w} (\boldsymbol{e}_\theta \otimes \boldsymbol{e}_\theta + \boldsymbol{e}_\phi \otimes \boldsymbol{e}_\phi) \right] \tag{29}$$

  where $w = 2\alpha/(2\alpha + \epsilon)$ and $\epsilon = \pm 1$ for $A_1 \gtrless 0$.

- The deviatoric approximation $\boldsymbol{\sigma}_2$ in cylindrical coordinates $\{\underline{e}_\rho, \underline{e}_\varphi, \underline{e}_z\}$

$$\boldsymbol{\sigma}_2 = A_2 \left(\underline{e}_\rho \otimes \underline{e}_\rho + \underline{e}_\varphi \otimes \underline{e}_\varphi - 2\underline{e}_z \otimes \underline{e}_z \right) \tag{30}$$

  The stress $\boldsymbol{\sigma}_1$ satisfies the void boundary condition ($\boldsymbol{\sigma} \cdot \underline{n} = \underline{0}$), but the one $\boldsymbol{\sigma}_2$ does not. In order to overcome this imperfection, a new term $\boldsymbol{\sigma}_3$ is added to ensure that: $\boldsymbol{\sigma} \cdot \underline{n} = (\boldsymbol{\sigma}_1 + \boldsymbol{\sigma}_2 + \boldsymbol{\sigma}_3) \cdot \underline{n} = \underline{0}$.

- The additional local stress field $\boldsymbol{\sigma}_3$

$$\boldsymbol{\sigma}_3 = S(r)\, A_2 \left[1 + 3\cos(2\theta) \right] \mathbf{1} + K(r)\, A_2 \sin(2\theta)(\underline{e}_r \otimes \underline{e}_\theta + \underline{e}_\theta \otimes \underline{e}_r) \tag{31}$$

  where $S(r) = \frac{\sqrt{15}}{30} \frac{a^{3/2}}{r^{3/2}} \left(-9 \sin\left(\frac{22}{2} \sqrt{15} \ln(\frac{a}{r}) \right) + \sqrt{15} \cos\left(\frac{\sqrt{15}}{2} \ln(\frac{a}{r}) \right) \right)$,
  $K(r) = \frac{1}{10} \frac{a^{3/2}}{r^{3/2}} \left(-15 \cos\left(\frac{\sqrt{15}}{2} \ln(\frac{a}{r}) \right) - 7\sqrt{15} \sin\left(\frac{\sqrt{15}}{2} \ln(\frac{a}{r}) \right) \right)$. A_1 and A_2 are constant parameters which need to be determined.

Finally the local terms σ_{eq} and σ_m used in the equation (1) can be calculated from $\boldsymbol{\sigma}$:

$$\sigma_m = \frac{A_1}{3\alpha}\left[1 - \left(\frac{a}{r}\right)^{3w}(1-w)\right] + S(r)\left[1 + 3\cos(2\theta)\right]A_2 \tag{32}$$

$$\sigma_{eq} = \sqrt{\left(\frac{w}{2\alpha}\right)^2\left(\frac{a}{r}\right)^{6w}A_1^2 + \frac{3A_1A_2w}{4\alpha}\left[1 + 3\cos(2\theta)\right]\left(\frac{a}{r}\right)^{3w} + Z_2(r,\theta)A_2^2} \tag{33}$$

where $Z_2(r,\theta) = \left[9 + 3K(r)\sin^2(2\theta)(K(r)+3)\right]$.

5.3. Macroscopic yield criteria based on the SVH mathod with the stress field $\boldsymbol{\sigma} = \boldsymbol{\sigma}_1 + \boldsymbol{\sigma}_2 + \boldsymbol{\sigma}_3$

With the relationship between $\boldsymbol{\sigma}$ and $\boldsymbol{\Sigma}$: $\boldsymbol{\Sigma} = \frac{1}{\Omega}\int_\Omega \boldsymbol{\sigma} dV$, the macroscopic stress tensor takes the following form:

$$\boldsymbol{\Sigma} = \left(\frac{1-f^w}{3\alpha}\right)A_1\mathbf{1} + Z_1A_2(\underline{e}_1\otimes\underline{e}_1 + \underline{e}_2\otimes\underline{e}_2 - 2\underline{e}_3\otimes\underline{e}_3) \tag{34}$$

where $Z_1 = 1 - \frac{\sqrt{15f}}{25}\sin\left(\frac{\sqrt{15}}{6}\ln(f)\right) - \sqrt{f}\cos\left(\frac{\sqrt{15}}{6}\ln(f)\right)$.

The macroscopic mean stress Σ_m and the equivalent stress Σ_{eq} can be easily obtained from (34):

$$\Sigma_m = \frac{1-f^w}{3\alpha}A_1, \qquad \Sigma_{eq} = 3Z_1|A_2| \tag{35}$$

By combining the expressions of (32), (33) and (34), the searched yield function can be computed as:

$$\frac{1}{|\Omega|}\int_{\Omega_M} f(\boldsymbol{\sigma})dV = \frac{3}{4\pi b^3}\int_a^b\int_0^\pi\int_0^{2\pi}\left[\sigma_{eq}(\boldsymbol{\Sigma}) + 3\alpha\sigma_m(\boldsymbol{\Sigma}) - \sigma_0\right]r^2\sin(\theta)d\varphi d\theta dr \le 0 \tag{36}$$

With the expression in (34), one can get:

$$\frac{3}{4\pi b^3}\int_a^b\int_0^\pi\int_0^{2\pi}\left[3\alpha\sigma_m(\boldsymbol{\Sigma}) - \sigma_0\right]r^2\sin(\theta)d\varphi d\theta dr = 3\alpha\Sigma_m - (1-f)\sigma_0 \tag{37}$$

Due to the complex of the parameter $Z_2(r,\theta)$ in the term σ_{eq}, it is not easy to get an explicit solution for the part $\frac{1}{|\Omega|}\int_{\Omega_M}\sigma_{eq}(\boldsymbol{\Sigma})dV$ in the equation (36).

For the purpose to facilitate the integral calculation and to get an closed form expression, the parameter $Z_2(r,\theta)$ here is approximated by a constant $Z_2(f)$. To do this, the studied Drucker-Prager criterion of the solid phase will be relaxed as: $F(\boldsymbol{\sigma}) = \sigma_e^2 - \tilde{\sigma}_0^2 = 0$, with $\tilde{\sigma}_0 = 3\alpha\sigma_m - \sigma_0$. Then, equation (36) reduces to: $\frac{3}{4\pi b^3}\int_a^b\int_0^\pi\int_0^{2\pi}(\sigma_e^2 - \tilde{\sigma}_0^2)r^2\sin(\theta)d\varphi d\theta dr \le 0$ which

can be solved analytically. According to the coefficient of parameter A_2, the approximated parameter $Z_2(f)$ can be calculated:

$$Z_2(r,\theta) \simeq Z_2(f) = 9\frac{1+\frac{11}{25}f-\frac{64}{75}f\ln(f)-2\sqrt{f}T+\frac{34}{375}fU}{1-f} \tag{38}$$
$$U = \sqrt{15}\sin\left(\frac{\sqrt{15}}{3}\ln(f)\right)+5\cos\left(\frac{\sqrt{15}}{3}\ln(f)\right), T = \frac{\sqrt{15}}{25}\sin\left(\frac{\sqrt{15}}{6}\ln(f)\right)+\cos\left(\frac{\sqrt{15}}{6}\ln(f)\right)$$

By adopting this simplification, the macroscopic yield function for the studied material can be derived:

$$\frac{\sqrt{Z_2}}{3Z_1}\frac{\Sigma_{eq}}{\sigma_0}\left[{}_2F_1(-\tfrac{1}{2},-\tfrac{1}{2w};1-\tfrac{1}{2w},-\beth^2)-f\ {}_2F_1(-\tfrac{1}{2},-\tfrac{1}{2w};1-\tfrac{1}{2w},-\tfrac{\beth^2}{f^{2w}})\right]+3\alpha\frac{\Sigma_m}{\sigma_0}-(1-f)\le 0 \tag{39}$$

in which $\beth = \left[\frac{9wZ_1}{2\sqrt{Z_2}(f^{-w}-1)}\frac{\Sigma_m}{\Sigma_{eq}}\right]$, the parameters Z_1 and Z_2 are given in Equations (34) and (38).

As given in Figure 7, the strength surface predicted by (39) (orange dashed line) is below that given by (13). It is not very precise in the compression zone when the frictional parameter α is high. But its accuracy is good for low values of α.

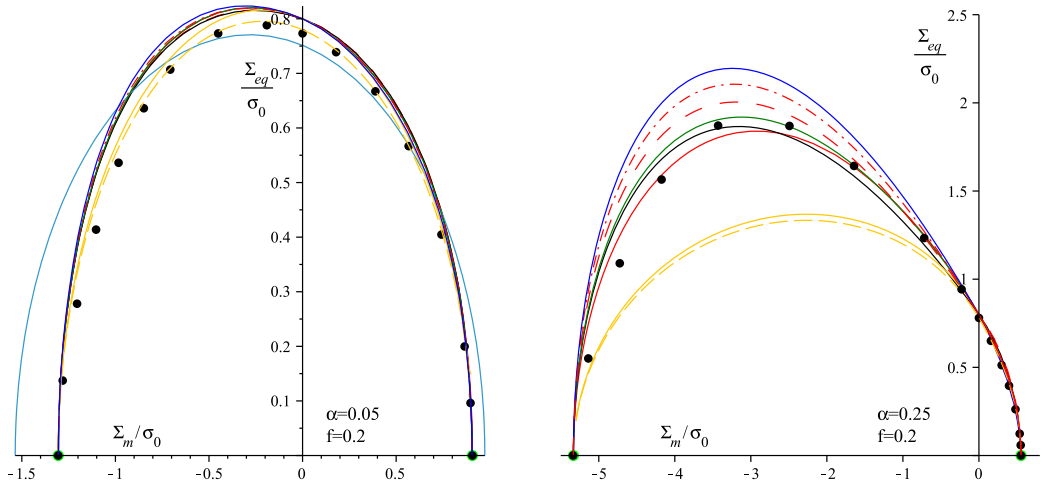

(a) $f = 0.2$, $\alpha = 0.05$ (b) $f = 0.2$, $\alpha = 0.25$

Figure 7: Comparisons of yield surfaces predicted by criteria (7)-black line, (8)-skyblue line, (9)-red solid line, (11) with Θ_1- red dashdot line, (11) with Θ_2-red dash line, (12)-green line, (15)-blue line, (13)-orange line, (39)-orange dashed line and FEM solutions with different α, $f = 0.2$.

5.4. New prediction of $\frac{\Sigma_{eq}}{\sigma_0}$ in pure shear loading ($\frac{\Sigma_m}{\sigma_0} = 0$)

As shown in Figure 7(a) with $f = 0.2$, the prediction of $\frac{\Sigma_{eq}}{\sigma_0}$ given by the criterion (39) is between $(1-f)$ and $\frac{1-f}{\sqrt{1+\frac{2}{3}f}}$ and coincides well with FEM results. It is then worth to study

in depth the value of $\frac{\Sigma_{eq}}{\sigma_0} = \frac{3Z_1}{\sqrt{Z_2}}$ provided by (39) with different f. Figure 8 illustrates the comparisons of $\frac{3Z_1}{\sqrt{Z_2}}$, $(1-f)$, $\frac{1-f}{\sqrt{1+\frac{2}{3}f}}$ and FEM results for the full range of porosity $0 < f < 1$. One can see a good agreement between the prediction $\frac{\Sigma_{eq}}{\sigma_0} = \frac{3Z_1}{\sqrt{Z_2}}$ provided by the new criterion and the FEM results.

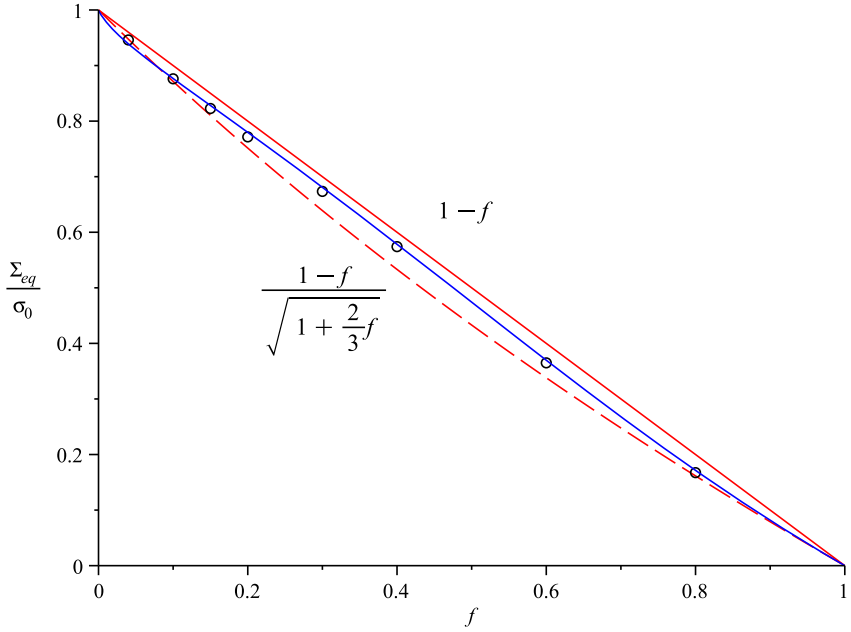

Figure 8: Comparisons between $\frac{\Sigma_{eq}}{\sigma_0}$ given by existing criteria and the one of FEM for pure deviatoric loading ($\frac{\Sigma_m}{\sigma_0} = 0$): Dashed line: $\frac{1-f}{\sqrt{1+2f/3}}$; Red line : $1-f$; Blue line: $\frac{3Z_1}{\sqrt{Z_2}}$.

6. A new macroscopic yield criterion and its validation by FEM results

Based on the comparisons between the main existing yield criteria and the new FEM numerical results in section 3 and the new value of $\frac{\Sigma_{eq}}{\sigma_0}$ for pure shear loading, a new macroscopic yield criterion will be derived in this section by adopting the strategy used in the [21, 20] and [16] to derive an explicit expression of yield criterion by considering some special cases.

In the hydrostatic loading ($\Sigma_{eq} = 0$), the exact solution can be derived (6), which can be expressed in the following general form:

$$2f\cosh\left[\frac{2\alpha + sgn(\Sigma_m)}{2\alpha}\ln(1 - 3\alpha\frac{\Sigma_m}{\sigma_0})\right] - 1 - f^2 = 0 \tag{40}$$

According to (40), the searched macroscopic yield criterion can be expressed in the following form:

$$\left(\frac{\Sigma_{eq}/\sigma_0}{B}\right)^2 + 2f\cosh\left[\frac{2\alpha + sgn(\Sigma_m)}{2\alpha}\ln(1-3\alpha\frac{\Sigma_m}{\sigma_0})\right] - 1 - f^2 = 0 \tag{41}$$

When the porosity is vanished, the searched macroscopic criterion should be reduced to the local one (1): $\frac{\Sigma_{eq}}{\sigma_0} + 3\alpha\frac{\Sigma_m}{\sigma_0} - 1 = 0$. With these conditions, one can get

$$\lim_{f\to 0} B = 1 - 3\alpha\frac{\Sigma_m}{\sigma_0} \tag{42}$$

In the pure shear loading ($\Sigma_m = 0$), the new value of $\frac{\Sigma_{eq}}{\sigma_0} = \frac{3Z_1}{\sqrt{Z_2}}$ will be adopted in the new searched criterion. This leads to:

$$B = \frac{3Z_1}{\sqrt{Z_2}(1-f)}, \quad \text{when} \quad \Sigma_m = 0 \tag{43}$$

As considered in [16], the searched yield criterion should satisfy the following condition when $\alpha = \frac{1}{2}$ and $\Sigma_m \le 0$ with the new value of $\frac{\Sigma_{eq}}{\sigma_0}$:

$$\frac{\Sigma_{eq}^2/\sigma_0^2}{\left[\frac{3Z_1}{\sqrt{Z_2}(1-f)} - \frac{3\Sigma_m}{2\sigma_0(1-f)}\right]^2} + 2f - (1+f^2) = 0 \tag{44}$$

which means $\lim_{\alpha\to\frac{1}{2},\Sigma_m\le 0} B = \frac{3Z_1}{\sqrt{Z_2}(1-f)} - \frac{3\Sigma_m}{2\sigma_0(1-f)}$.

Based on the comparisons of the existing yield criterion and satisfying the above requirements, a new heuristic macroscopic criterion is proposed in the following form for porous materials with a Drucker-Prager solid matrix and spherical void::

$$\left(\frac{\frac{\Sigma_{eq}}{\sigma_0}}{\frac{3Z_1}{\sqrt{Z_2}(1-f)} - \frac{3\alpha}{1+\gamma\ln(1+sf)}\frac{\Sigma_m}{\sigma_0}}\right)^2 + 2f\cosh\left[\frac{sign(\Sigma_m)+2\alpha}{2\alpha}\ln\left(1-3\alpha\frac{\Sigma_m}{\sigma_0}\right)\right] - 1 - f^2 = 0 \tag{45}$$

This criterion satisfies all the special conditions considered in [20] and [16].

The new criterion (45) is evaluated in Figures 9 and 10 by the new finite element solutions carried out in this work. Different porosity $f = 0.04, 0.1, 0.15, 0.2, 0.3, 0.4$ and frictional parameter $\alpha = 0, 0.05, 0.1, 0.15, 0.2, 0.25, 0.3$ (the corresponding friction angles are $\phi = 0, 8.53°, 16.70°, 24.23°, 30.96°, 36.87°, 41.99°$) are considered for a wide validation. The criterion (45) find well the hydrostatic analytical solutions (green points). The values of pure shear strength $\frac{\Sigma_{eq}}{\sigma_0}$ are well predicted for all values of porosity. The influences of porosity and frictional parameter on the overall strength behavior are better predicted by (45) than the previous ones.

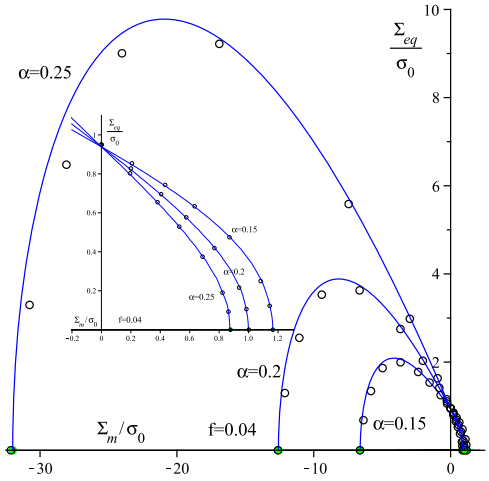

(a) $f = 0.04,\ \alpha = 0.15,\ 0.2,\ 0.25$

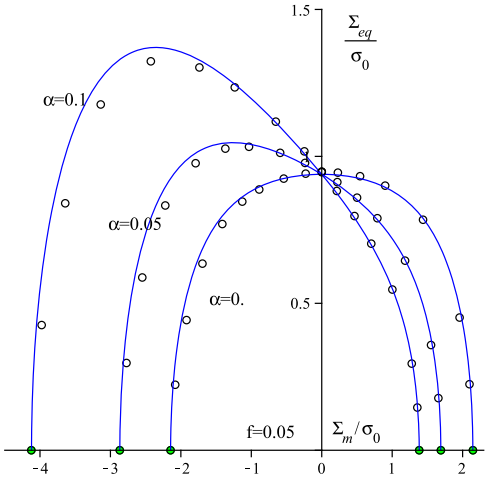

(b) $f = 0.04,\ \alpha = 0.0,\ 0.05,\ 0.1$

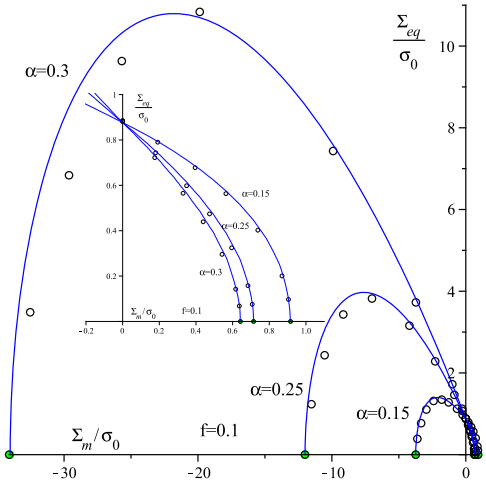

(c) $f = 0.1,\ \alpha = 0.15,\ 0.25,\ 0.3$

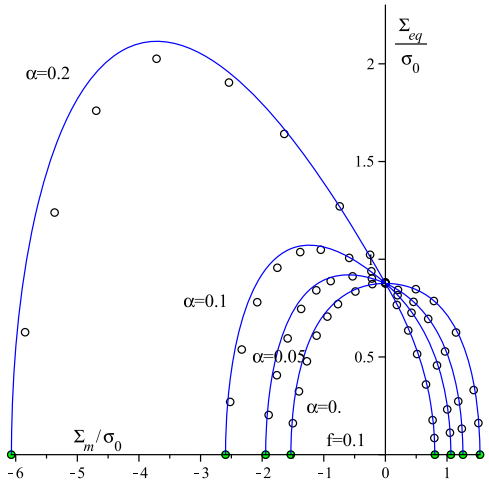

(d) $f = 0.1,\ \alpha = 0.0,\ 0.05,\ 0.1,\ 0.2$

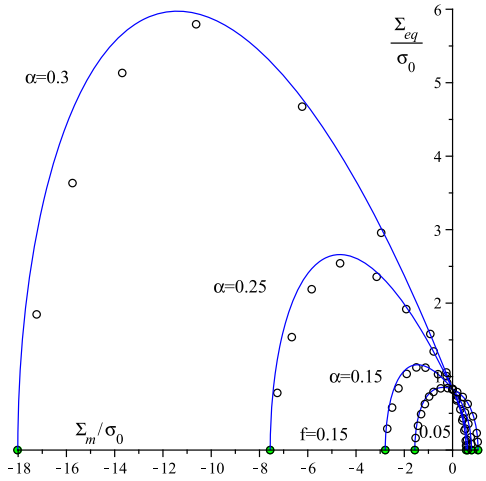

(e) $f = 0.15,\ \alpha = 0.05,\ 0.15,\ 0.25,\ 0.3$

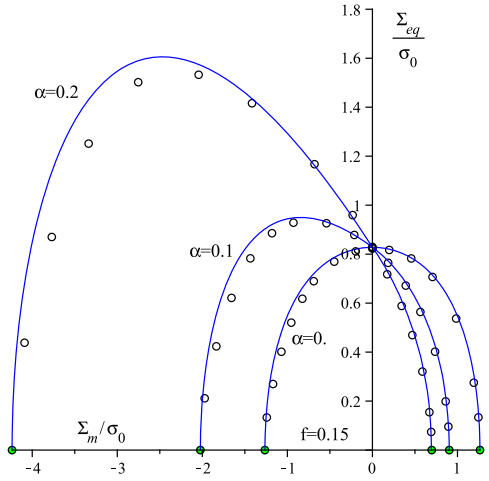

(f) $f = 0.15,\ \alpha = 0.0,\ 0.1,\ 0.2$

Figure 9: Comparisons between yield surfaces predicted by new criterions (blue line) and FEM solutions (circles) with different α and f, green points: exact solution in pure hydrostatic loading.

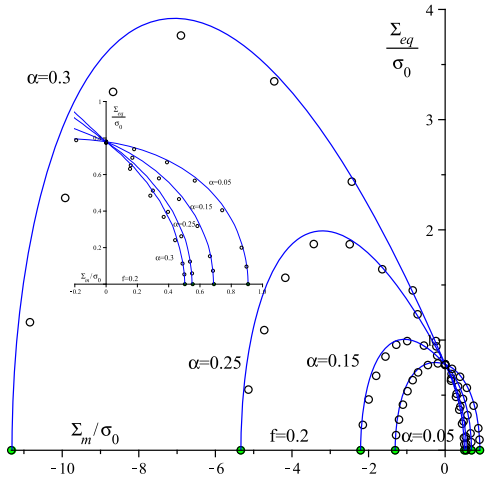

(a) $f = 0.2,\ \alpha = 0.05,\ 0.15,\ 0.25,\ 0.3$

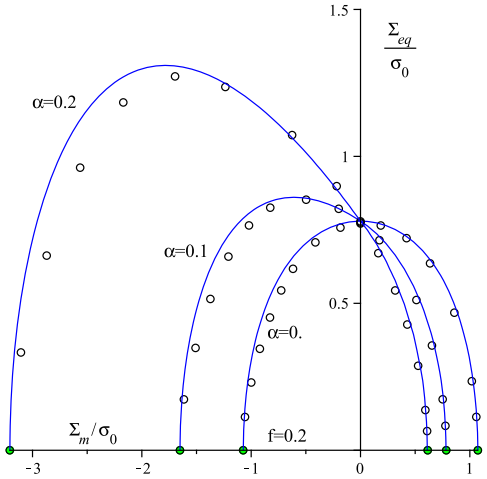

(b) $f = 0.2,\ \alpha = 0.0,\ 0.1,\ 0.2$

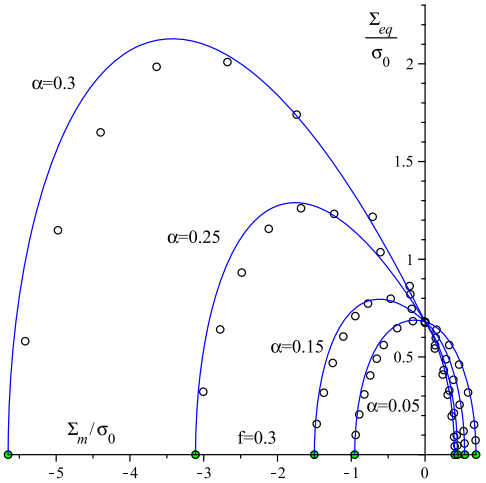

(c) $f = 0.3,\ \alpha = 0.05,\ 0.15,\ 0.25,\ 0.3$

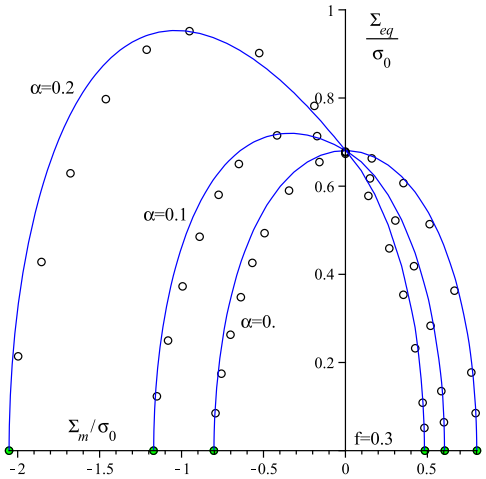

(d) $f = 0.3,\ \alpha = 0.0,\ 0.1,\ 0.2$

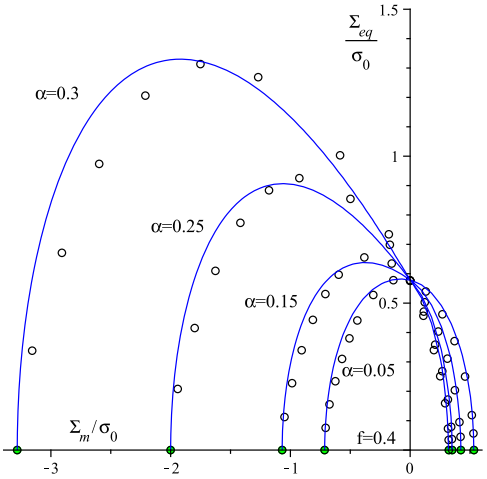

(e) $f = 0.4,\ \alpha = 0.05,\ 0.15,\ 0.25,\ 0.3$

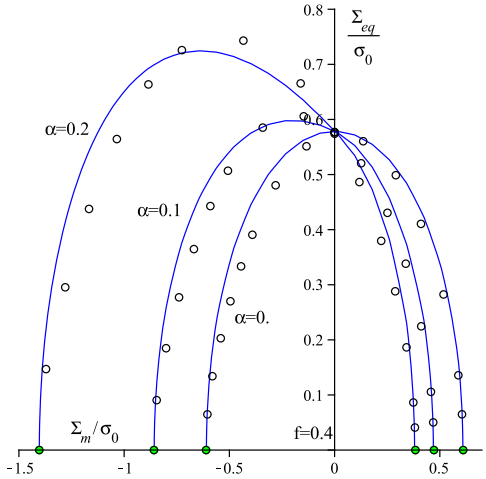

(f) $f = 0.4,\ \alpha = 0.0,\ 0.1,\ 0.2$

Figure 10: Comparisons between yield surfaces predicted by new criterions (blue line) and FEM solutions (circles) with different α and f, green points: exact solution in pure hydrostatic loading.

The relative errors between the FEM numerical results and yield surfaces predicted by the new macroscopic yield criterion (45) are illustrated in Figure 11 and 12 as a function of macroscopic stress triaxiality T, for different porosity with $\alpha = 0.15$ and different frictional parameter with $f = 0.15$. When $-1.33 < T < -4.33$ for the compressive loading and $1.83 < T < 0.58$ for the tensile loading, one finds the maximal errors.

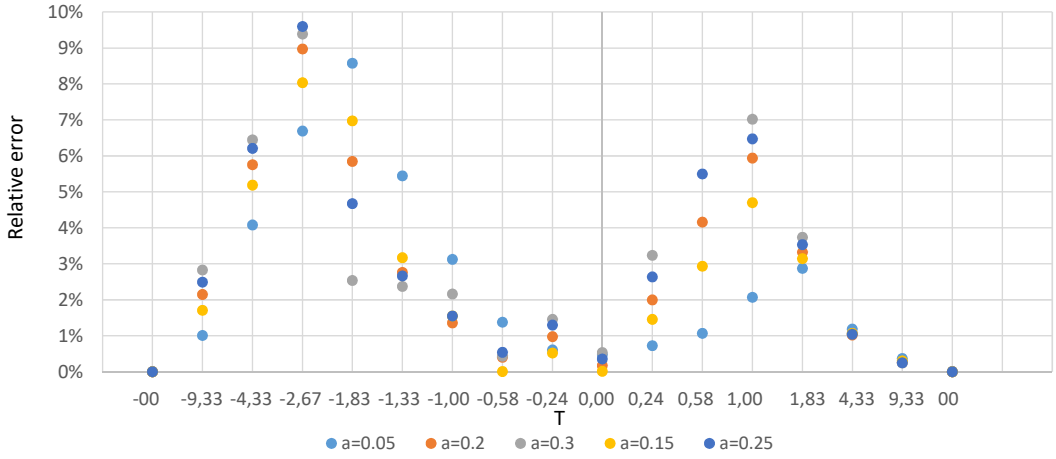

Figure 11: Relative errors between the numerical results and yield surfaces given by (45) with different frictional parameter α, $f = 0.15$.

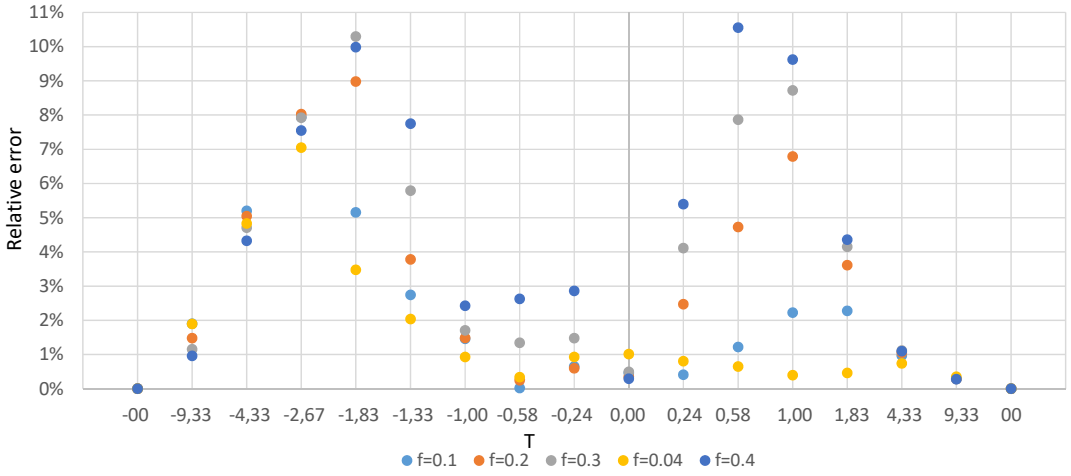

Figure 12: Relative errors between the numerical results and yield surfaces given by (45) with different porosity f, $\alpha = 0.15$.

- Special case for a porous material with a von Mises type marix

It is interesting to consider the special case of the macroscopic yield criterion (45) for a porous material with a pressure-independent (von Mises type) matrix, $\alpha = 0$. The yield function (45) reduces to the following form:

$$\frac{\Sigma_{eq}^2/\sigma_0^2}{\frac{9Z_1^2}{Z_2(1-f)^2}} + 2f\cosh\left(\frac{3\Sigma_m}{2\sigma_0}\right) - 1 - f^2 = 0 \tag{46}$$

For the purpose of validation, the yield surfaces predicted by (46) is assessed by the numerical upper and lower bounds [46, 44] and FEM results [6] in Figures 13-15 for different porosity $f = 0.01$, 0.064 and 0.1. The theoretical coinsides well with the numerical results, especially for the hydrostatic and deviatoric loadings. There is a good agrement. The yield criterion (46) improves the Gurson's one in deviatoric loading.

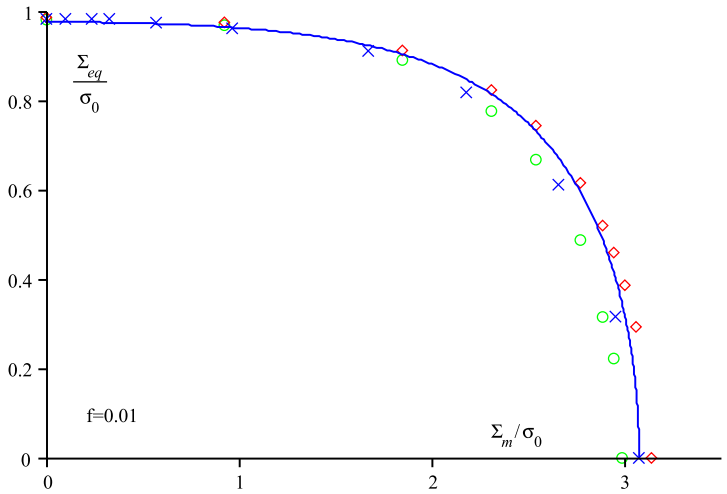

Figure 13: Comparisons between the yield surface predicted by 46, numerical bounds [46](red point: upper bound; green point: lower bound) and FEM numerical results (cross point) [6], $f = 0.01$.

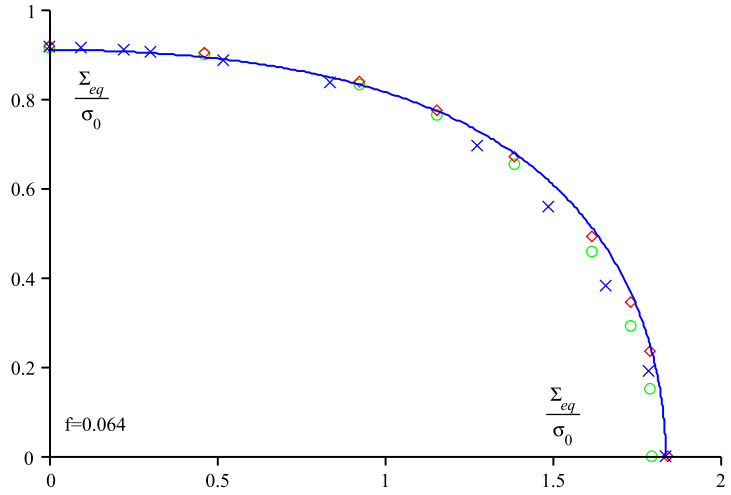

Figure 14: Comparisons between the yield surface predicted by 46, numerical bounds [46](red point: upper bound; green point: lower bound) and FEM numerical results (cross point) [6], $f = 0.064$.

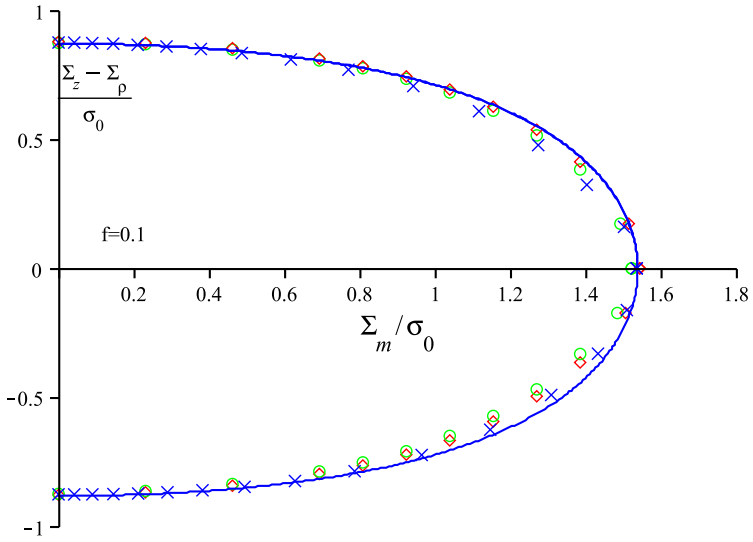

Figure 15: Comparisons between the yield surface predicted by 46, numerical bounds [44](red point: upper bound; green point: lower bound) and FEM numerical results (cross point) [6], $f = 0.1$.

7. Conclusions

This study has focused on the macroscopic strength function of porous geomaterials having a D-P matrix. We have provided in depth theoretical and numerical assessments of main existing criteria derived by different approach. A series of new numerical FEM solutions with a wide range of porosity and frictional parameter has been carried out in this work and treated as references for the validations. In particular, the influences of porosity and frictional parameters on the macroscopic strength have been investigated with the help of these numerical results. It is found that the macroscopic strength of the existing criteria for high loads with low triaxiality need to be improved. Especially, the prediction of deviatoric strength $\frac{\Sigma_{eq}}{\sigma_0}$ in pure shear loading are fully studied. Based on the theoretical and numerical assessments, a new value is derived in this work for the studied materials by using the SVH approach with strict statically admissible stress fields. Taking advantage of these comparisons, a new approximated yield criterion is established. It demonstrates that this yield criterion clearly improves the analytical predictions of previous criteria, and also for the special case for the porous material with von Mises type matrix.

Acknowledgement

This study was supported by the National Natural Science Foundation of China (Grant No. 11902069).

Appendix A. Recapitulation of the existing macroscopic criteria of porous material with Drucker-Prager matrix

Recapitulation of the existing macroscopic criteria of porous material with Drucker-Prager matrix

Reference	Criterion	Method	E. S.($\Sigma_{eq}=0$)	$\frac{\Sigma_{eq}}{\sigma_0}(\Sigma_m=0)$	Pore	Flow rule
Lazzeri and Bucknall(1993)[23]	Eq. (3)	Modification of Gurson's criterion	×	$1-f$	Sphere	Associated
Jeong and Pan(1995) [21]	Eq. (4)	Based on some special cases	T-√, C-×	$1-f$	Sphere	Associated
Al-Abduljabbar and Pan (1999)[1]	Eq. (5)	Modification based on Eq.(4)	T-√, C-×	$1-f$	Sphere	Associated
Jeong (2002)[20]	Eq. (7)	Based on some special cases	√	$1-f$	Sphere	Associated
Barthélémy and Dormieux(2003)[3]	Eq. (8)	Modified secant method	×	$\frac{1-f}{\sqrt{1+\frac{2}{3}f}}$	Sphere	Associated
Guo et al.(2008) [16]	Eq. (9)	Limit analysis approach	√	$1-f$	Sphere	Associated
Guo et al.(2008) [16]	Eq. (11)	Based on some special cases	√	$1-f$	Sphere	Associated
Durban et al.(2010)[13]	Eq. (12)	Expanding yield function in powers of f	√	$1-f$	Sphere	Associated
Cheng et al.(2013)[8]	Eq. (13)	Stress variational method	√	$1-f$	Sphere	Associated
Shen et al.(2017) [37]	Eq. (14)	Limit analysis approach	×	$1-f$	Spheroid	Associated
Shen et al.(2017) [37]	Eq. (15)	Special case of Eq. (14)	√	$1-f$	Sphere	Associated
Maghous et al.(2009)[24]	Eq. (8)	Modified secant method	×	$\frac{1-f}{\sqrt{1+\frac{2}{3}f}}$	Sphere	Non-Associated
Cheng et al.(2015)[9]	Eq. (18)	Bipotential based limit analysis	√	$1-f$	Sphere	Non-Associated

Appendix B. Parameters used in the macroscopic criterion (14)

The parameters used in the equation (14):

$$
\begin{cases}
\Upsilon = \dfrac{\alpha}{(1-f)}, \quad \tau = \dfrac{\Upsilon}{1-\Upsilon(3\alpha_2-1)\frac{\Sigma_q}{\sigma_0}} \\
\Psi = \dfrac{(3\alpha_2-1)\frac{\Sigma_q}{\sigma_0} + \tau(3\alpha_2-1)^2\frac{\Sigma_{eq}^2}{\sigma_0^2} - \frac{3(1-f)\frac{\Sigma_m}{\sigma_0}}{(1-f)-3\alpha\frac{\Sigma_m}{\sigma_0}}}{\tau(3\alpha_2-1)\left(\Upsilon(3\alpha_2-1)(\frac{\eta(3\alpha_2-1)}{3}-1)(\frac{\Sigma_{eq}^2}{\sigma_0^2}-\frac{\Sigma_q^2}{\sigma_0^2}) - \frac{\Sigma_q}{\sigma_0}\right) - 1} \\
\mathfrak{R} = 1 - \Psi\Upsilon(\dfrac{\eta(3\alpha_2-1)}{3}-1), \quad \Sigma_s = \dfrac{\Psi\eta}{3-3\Upsilon(3\alpha_2-1)\frac{\Sigma_q}{\sigma_0}} \\
\Sigma_q = \boldsymbol{\Sigma} : \boldsymbol{Q} \\
\Gamma = \dfrac{(3\alpha_2-1)\frac{\Sigma_q}{\sigma_0} + \tau(3\alpha_2-1)^2\frac{\Sigma_{eq}^2}{\sigma_0^2} + \frac{2\alpha+sgn(\Sigma_m)}{2\alpha}\ln\left[1-3\alpha\frac{\Sigma_m}{\sigma_0}\Delta\right]sgn(\Sigma_m)}{\tau(3\alpha_2-1)\left(\Upsilon(3\alpha_2-1)(\frac{\eta(3\alpha_2-1)}{3}-1)(\frac{\Sigma_{eq}^2}{\sigma_0^2}-\frac{\Sigma_q^2}{\sigma_0^2}) - \frac{\Sigma_q}{\sigma_0}\right) - 1} \\
\Delta = \frac{1+sgn(\Sigma_m)}{2} + \left(\frac{1}{1-\zeta} - \eta\right)\frac{1-sgn(\Sigma_m)}{2}
\end{cases}
\tag{B.1}
$$

$$
p^2 = \frac{3}{2}\frac{(1+g)(f+g)}{f(1-f)}\left\{6\left[\alpha_1(1-\alpha_1) - f\alpha_2(1-\alpha_2)\right] + 2\left[(1-\alpha_1) - f(1-\alpha_2)\right]\right\} \tag{B.2}
$$

$$
\eta = \frac{9(1+g)(f+g)(\alpha_2-\alpha_1)}{p^2(1-f)} \tag{B.3}
$$

$$
\zeta = \frac{9(1+g)(f+g)(\alpha_2-\alpha_1)^2}{p^2(1-f)^2} \tag{B.4}
$$

$$
\chi = \frac{4}{3\alpha_1 - 1} \tag{B.5}
$$

$$
w = \frac{2(1+g)(f+g)(\alpha_2-\alpha_1)}{\chi g(1-f)} \tag{B.6}
$$

$$
\alpha(e) = \begin{cases} \dfrac{1-e^2}{e^3}\operatorname{arctanh}\{e\} - \dfrac{1-e^2}{e^2} \\ -\dfrac{\sqrt{1-e^2}}{e^3}\arctan\left\{\frac{e}{\sqrt{1-e^2}}\right\} + \dfrac{1}{e^2} \end{cases} \qquad \beta(e) = \begin{cases} (1-3\alpha)\frac{1}{e^2} & \text{(prolate)} \\ -(1-3\alpha)\frac{1-e^2}{e^2} & \text{(oblate)} \end{cases} \tag{B.7}
$$

where $\alpha_1 = \alpha(e_1)$, $\alpha_2 = \alpha(e_2)$ and $\beta_1 = \beta(e_1)$, $\beta_2 = \beta(e_2)$.

Appendix C. Parameter used in the macroscopic criterion (18)

The parameters Π_{C_0}, Π_{D_e}, $\hat{\Pi}_{C_0}$, $\hat{\Pi}_{D_e}$ and $\tilde{\gamma}$ are given as:

$$\mathcal{P} = {}_2F_1\left(-\frac{1}{2}, -\frac{\tilde{s}}{2}; 1-\frac{\tilde{s}}{2}; -\tau^2\right) - f\ {}_2F_1\left(-\frac{1}{2}, -\frac{\tilde{s}}{2}; 1-\frac{\tilde{s}}{2}; -\frac{\tau^2}{f^{2/\tilde{s}}}\right) \tag{C.1}$$

$$\Pi_{C_0} = \frac{\tau}{\tilde{s}/2-1}\left[{}_2F_1\left(\frac{1}{2}, 1-\frac{\tilde{s}}{2}; 2-\frac{\tilde{s}}{2}; -\tau^2\right) - f^{1-2/\tilde{s}}\ {}_2F_1\left(\frac{1}{2}, 1-\frac{\tilde{s}}{2}; 2-\frac{\tilde{s}}{2}; -\frac{\tau^2}{f^{2/\tilde{s}}}\right)\right] \tag{C.2}$$

$$\Pi_{D_e} = {}_2F_1\left(\frac{1}{2}, -\frac{\tilde{s}}{2}; 1-\frac{\tilde{s}}{2}; -\tau^2\right) - f\ {}_2F_1\left(\frac{1}{2}, -\frac{\tilde{s}}{2}; 1-\frac{\tilde{s}}{2}; -\frac{\tau^2}{f^{2/\tilde{s}}}\right) \tag{C.3}$$

$$\hat{\Pi}_{C_0} = \Pi_{C_0} + \frac{3\alpha\frac{\Sigma_m}{\sigma_0}}{1-f^\gamma}\left(\frac{f^\gamma}{s}I_{C_0} - \Pi_{C_0}\right) \tag{C.4}$$

$$\hat{\Pi}_{D_e} = \Pi_{D_e} + \frac{3\alpha\frac{\Sigma_m}{\sigma_0}}{1-f^\gamma}\left(\frac{f^\gamma}{s}I_{D_e} - \Pi_{D_e}\right) \tag{C.5}$$

$$I_{C_0} = \frac{2\tau}{\tilde{s}/s-2}\left[{}_2F_1\left(\frac{1}{2}, 1-\frac{\tilde{s}}{2s}; 2-\frac{\tilde{s}}{2s}; -\tau^2\right) - f^{1/s-2/\tilde{s}}\ {}_2F_1\left(\frac{1}{2}, 1-\frac{\tilde{s}}{2s}; 2-\frac{\tilde{s}}{2s}; -\frac{\tau^2}{f^{2/\tilde{s}}}\right)\right] \tag{C.6}$$

$$I_{D_e} = s\left[{}_2F_1\left(\frac{1}{2}, -\frac{\tilde{s}}{2s}; 1-\frac{\tilde{s}}{2}; -\tau^2\right) - f^{\frac{1}{s}}\ {}_2F_1\left(\frac{1}{2}, -\frac{\tilde{s}}{2s}; 1-\frac{\tilde{s}}{2s}; -\frac{\tau^2}{f^{2/\tilde{s}}}\right)\right] \tag{C.7}$$

$$\tau = \frac{2C_0}{\tilde{s}D_e}, \quad \tilde{s} = 1+2\epsilon\beta, \quad \tilde{\gamma} = \frac{2\epsilon\beta}{1+2\epsilon\beta} \tag{C.8}$$

Appendix D. Evaluations of the existing yield criteria by FEM results with different f and α

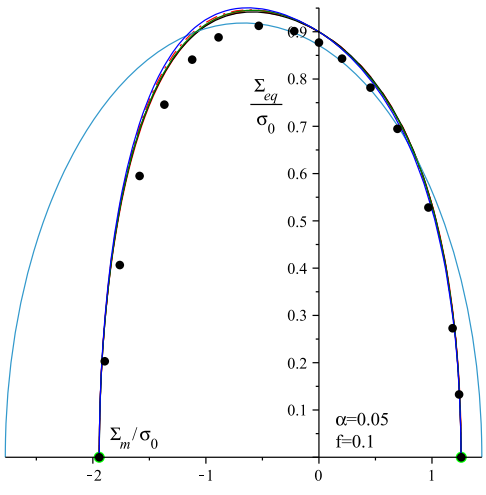

(a) $f = 0.1$, $\alpha = 0.05$

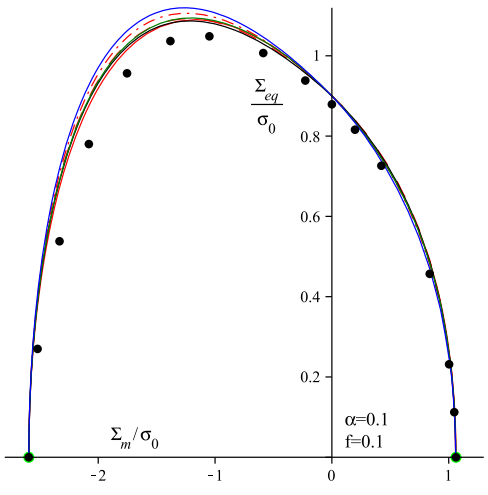

(b) $f = 0.1$, $\alpha = 0.1$

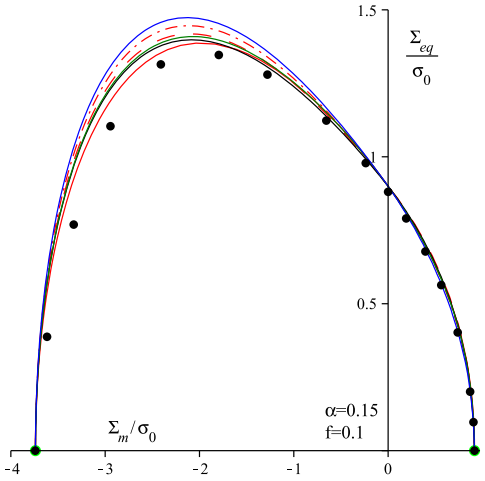

(c) $f = 0.1$, $\alpha = 0.15$

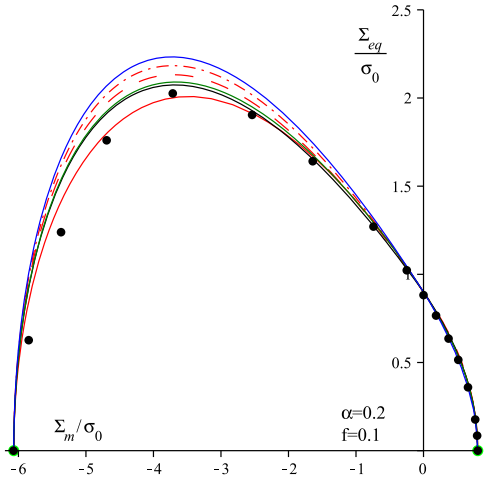

(d) $f = 0.1$, $\alpha = 0.2$

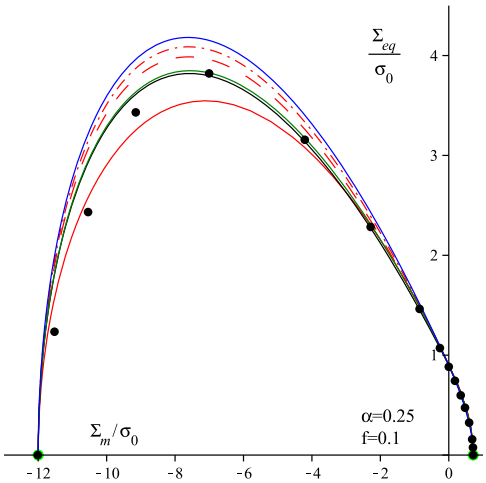

(e) $f = 0.1$, $\alpha = 0.25$

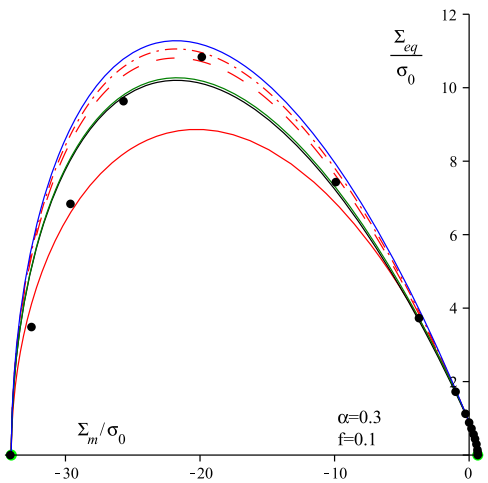

(f) $f = 0.1$, $\alpha = 0.3$

Figure D.16: Comparisons of yield surfaces predicted by criteria (7)-black line, (8)-skyblue line, (9)-red solid line, (11) with Θ_1- red dashdot line, (11) with Θ_2-red dash line, (12)-green line, (15)-blue line and FEM solutions with different α, $f = 0.1$.

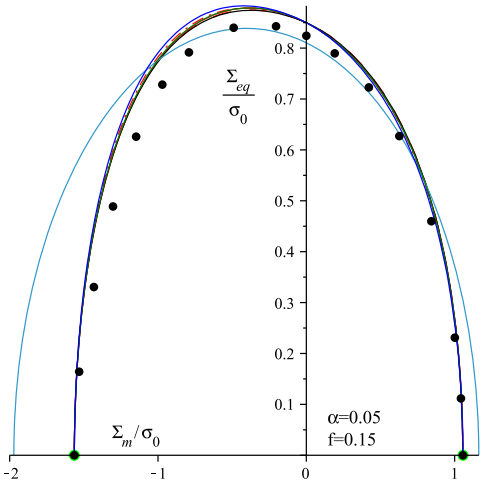

(a) $f = 0.15$, $\alpha = 0.05$

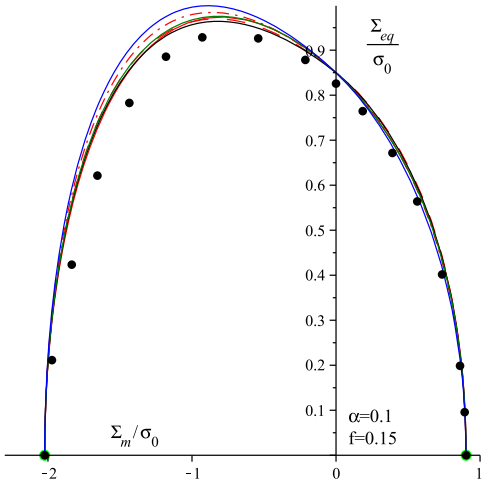

(b) $f = 0.15$, $\alpha = 0.1$

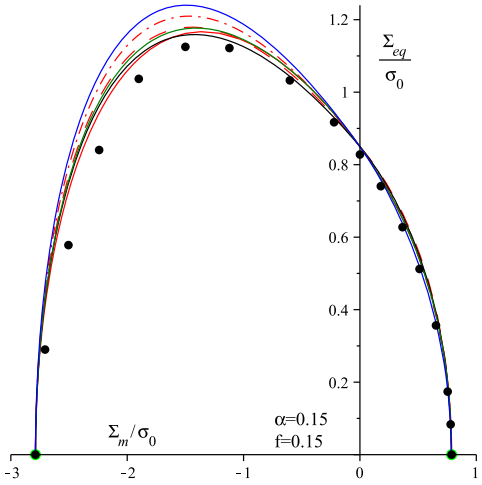

(c) $f = 0.15$, $\alpha = 0.15$

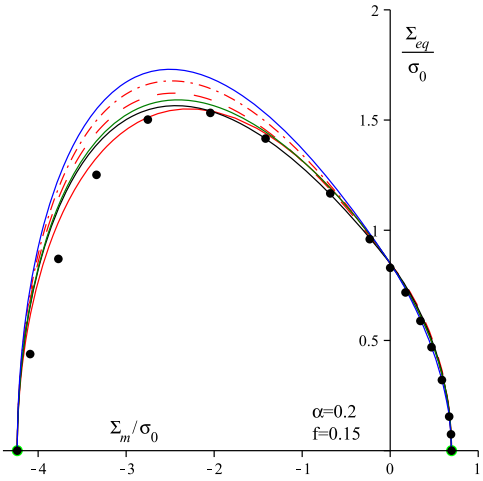

(d) $f = 0.15$, $\alpha = 0.2$

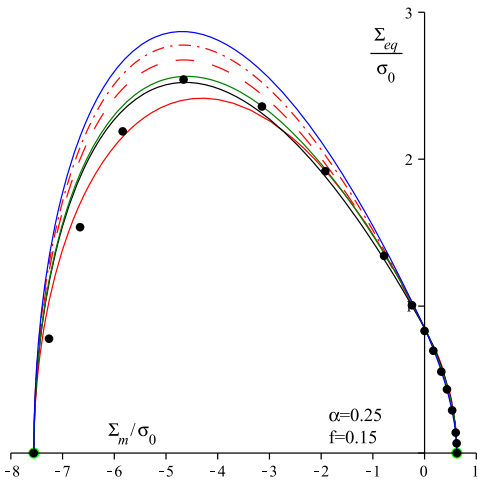

(e) $f = 0.15$, $\alpha = 0.25$

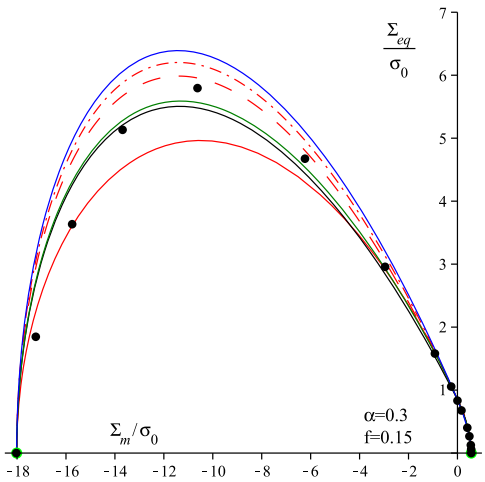

(f) $f = 0.15$, $\alpha = 0.3$

Figure D.17: Comparisons of yield surfaces predicted by criteria (7)-black line, (8)-skyblue line, (9)-red solid line, (11) with Θ_1- red dashdot line, (11) with Θ_2-red dash line, (12)-green line, (15)-blue line and FEM solutions with different α, $f = 0.15$.

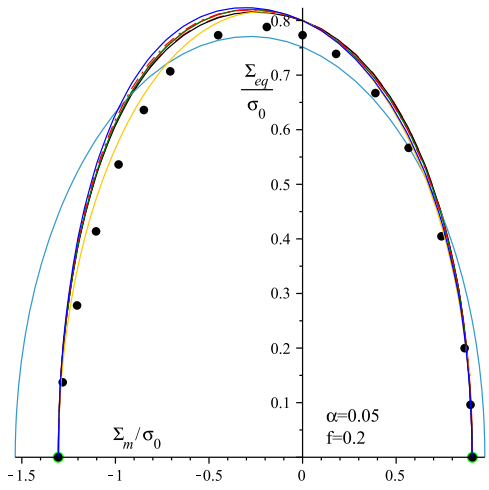

(a) $f = 0.2$, $\alpha = 0.05$

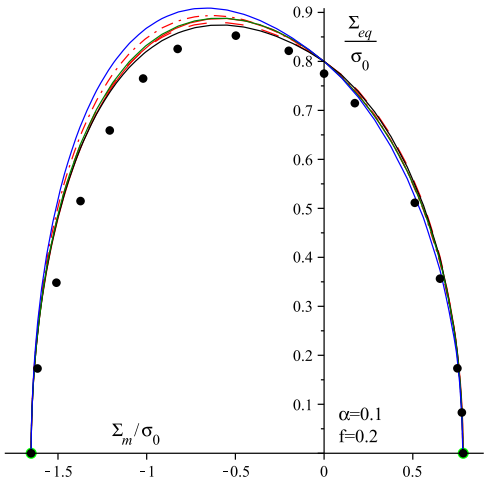

(b) $f = 0.2$, $\alpha = 0.1$

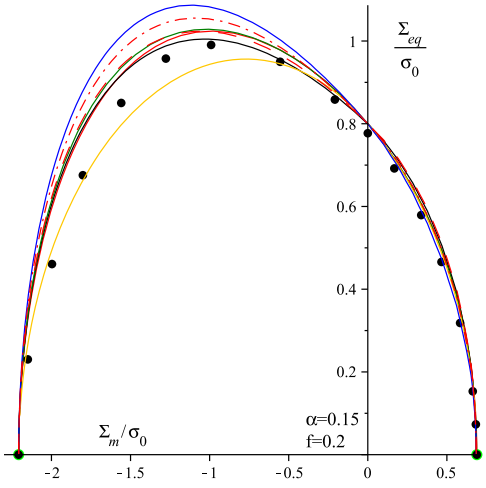

(c) $f = 0.2$, $\alpha = 0.15$

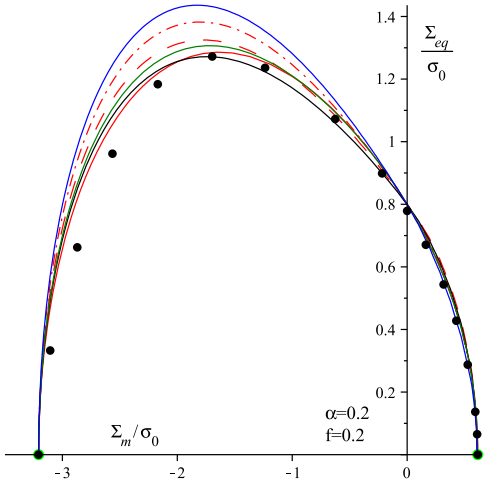

(d) $f = 0.2$, $\alpha = 0.2$

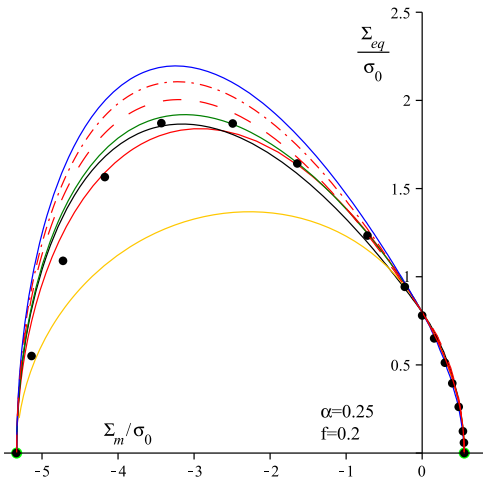

(e) $f = 0.2$, $\alpha = 0.25$

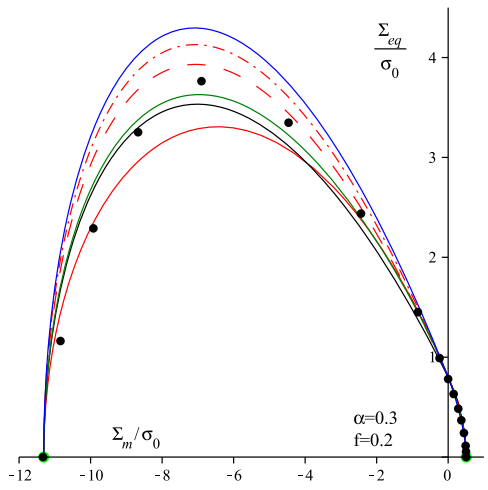

(f) $f = 0.2$, $\alpha = 0.3$

Figure D.18: Comparisons of yield surfaces predicted by criteria (7)-black line, (8)-skyblue line, (9)-red solid line, (11) with Θ_1- red dashdot line, (11) with Θ_2-red dash line, (12)-green line, (15)-blue line, (13)-orange line and FEM solutions with different α, $f = 0.2$.

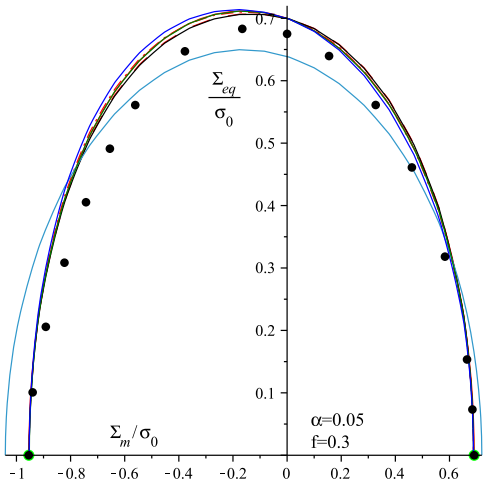

(a) $f = 0.3$, $\alpha = 0.05$

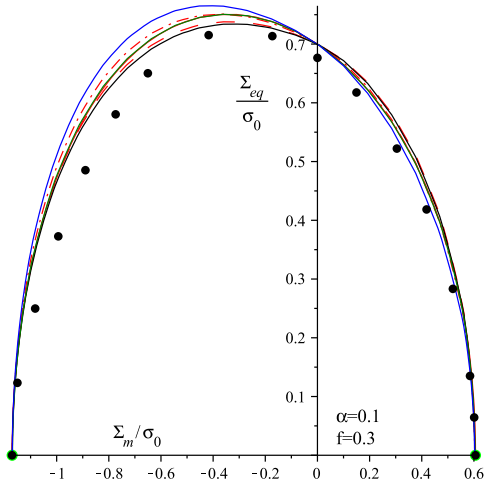

(b) $f = 0.3$, $\alpha = 0.1$

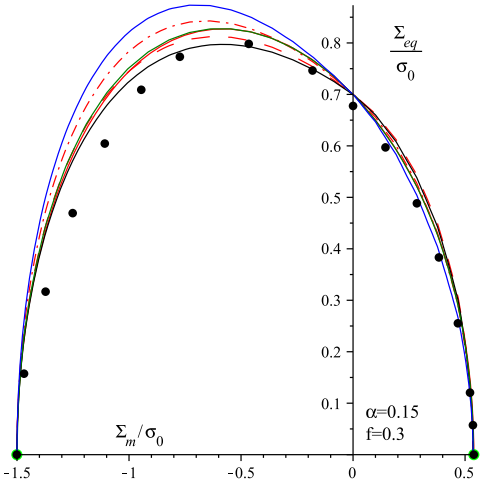

(c) $f = 0.3$, $\alpha = 0.15$

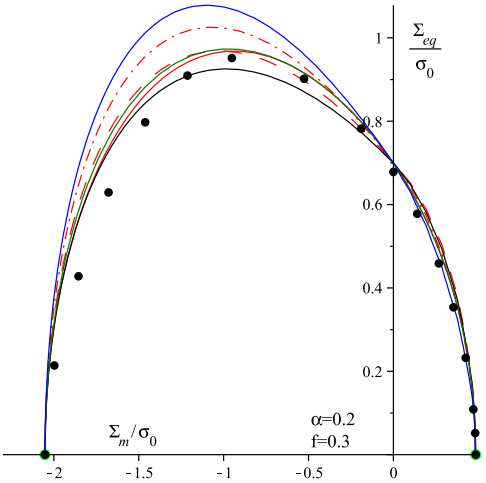

(d) $f = 0.3$, $\alpha = 0.2$

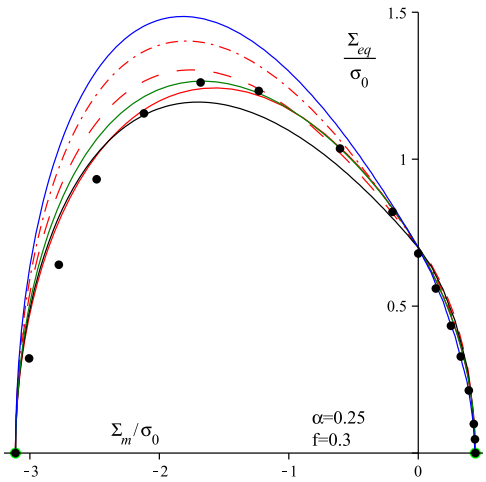

(e) $f = 0.3$, $\alpha = 0.25$

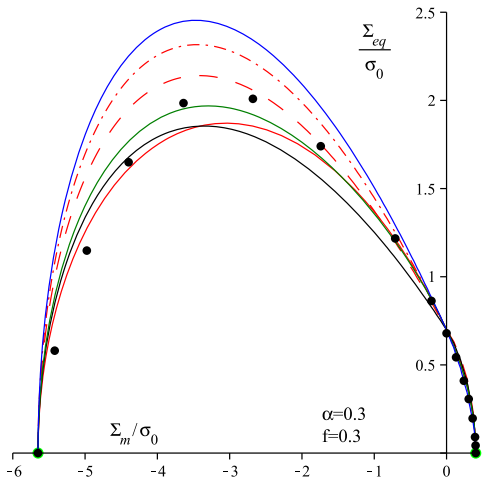

(f) $f = 0.3$, $\alpha = 0.3$

Figure D.19: Comparisons of yield surfaces predicted by criteria (7)-black line, (8)-skyblue line, (9)-red solid line, (11) with Θ_1- red dashdot line, (11) with Θ_2-red dash line, (12)-green line, (15)-blue line and FEM solutions with different α, $f = 0.3$.

References

[1] A. Al-Abduljabbar and J. Pan. Numerical analysis of notch-tip fields in rubber-modified epoxies. *Polymer Engineering and Science*, 39:662–675, 1999.

[2] E. E. Alonso, A. Gens, and A. Josa. A constitutive model for partially saturated soils. *Géotechnique*, 40(3):405–430, 1990.

[3] J.-F. Barthélémy and L. Dormieux. Détermination du critère de rupture macroscopique d'un milieu poreux par homogénéisation non linéaire. *C. R. Mecanique*, 331:271–276, 2003.

[4] François Bignonnet, Luc Dormieux, and Eric Lemarchand. Strength of a matrix with elliptic criterion reinforced by rigid inclusions with imperfect interfaces. *European Journal of Mechanics - A/Solids*, 52:95 – 106, 2015.

[5] S. Brach, L. Dormieux, D. Kondo, and G. Vairo. Nanoporous materials with a general isotropic plastic matrix: Exact limit state under isotropic loadings. *International Journal of Plasticity*, 89:1–28, 2017.

[6] L. Cheng, G. de Saxcé, and D. Kondo. A stress-based variational model for ductile porous materials. *International Journal of Plasticity.*, 55:133–151, 2013.

[7] L. Cheng and T. F. Guo. Void interaction and coalescence in polymeric materials. *Int. J. Solids Struct.*, 44:1787–1808, 2007.

[8] L. Cheng, Y. Jia, A Oueslati, G. De Saxcé, and D. Kondo. Approche variationnelle en contraintes du critère macroscopique d'un milieu poreux ductile ayant une matrice de drucker-prager. *21ème Congrès Français de Mécanique, Bordeaux*, 2013.

[9] L. Cheng, Y. Jia, A Oueslati, G. De Saxcé, and D. Kondo. A bipotential-based limit analysis and homogenization of ductile porous materials with non-associated drucker-prager matrix. *J.Mech.Phys.Solids*, 77:1–26, 2015.

[10] G. De Saxcé. Une généralisation de l'inégalité de fenchel et ses applications aux lois constitutives. *C. R. Acad. Sci. Paris Sér. II*, 314:125–129, 1992.

[11] G. De Saxcé and L. Bousshine. On the extension of limit analysis theorems to the non-associated flow rules in soils and to the contact with coulomb's friction. *In: XI Polish Conference on Computer Methods in Mechanics. Kielce, Poland*, pages 815–822, 1993.

[12] G. De Saxcé and Z.Q. Feng. New inequality and functional for contact friction: the implicit standard material approach. *Mech. Struct. Mach.*, 19:301–325, 1991.

[13] D. Durban, T. Cohen, and Y. Hollander. Plastic response ofporous solids with pressure sensitive matrix. *Mechanics Research Communications*, 37:636–641, 2010.

[14] M. Gologanu, J.B. Leblond, and J. Devaux. Approximate models for ductile metals containing non-spherical voids–cas of axisymmetric prolate ellipsoidal cavities. *J.Mech.Phys.Solids*, 41(11):1723–1754, 1993.

[15] M. Gologanu, J.B. Leblond, and J. Devaux. Approximate models for ductile metals containing non-spherical voids–cas of axisymmetric oblate ellipsoidal cavities. *ASME J.Eng. Mat. Tech.*, 116:290–297, 1994.

[16] T.F. Guo, J. Faleskog, and C.F. Shih. Continuum modeling of a porous solid with pressure sensitive dilatant matrix. *J. Mech. Phys. Solids*, 56:2188–2212, 2008.

[17] A.L. Gurson. Continuum theory of ductile rupture by void nucleation and growth: part1-yield criteria and flow rules for porous ductile media. *J. Engrg. Mater. Technol.*, 99:2–15, 1977.

[18] Z. He, L. Dormieux, and D. Kondo. Strength properties of a drucker-prager porous medium reinforced

by rigid particles. *International Journal of Plasticity*, 51:218 – 240, 2013.

[19] M. Hjiaj, J. Fortin, and G. De Saxcé. A complete stress update algorithm for the non-associated drucker-prager model including treatment of the apex. *Int. J. Eng. Sci.*, 41:1109–1143, 2003.

[20] H.Y. Jeong. A new yield function and a hydrostatic stress-controlled model for porous solids with pressure-sensitive matrices. *Int. J. Solids Struct.*, 39:1385–1403, 2002.

[21] H.Y. Jeong and J. Pan. A macroscopic constitutive law for porous solids with pressure-sensitive matrices and its implications to plastic flow localization. *Int. J. Solids Struct.*, 32:3669–3691, 1995.

[22] S.M. Keralavarma and A.A. Benzerga. A constitutive model for plastically anisotropic solids with non-spherical voids. *Journal of the Mechanics and Physics of Solids*, 58:874–901, 2010.

[23] A. Lazzeri and C.B. Bucknall. Dilatational bands in rubber toughened polymers. *Journal of Materials Science*, 28:6799–6808, 1993.

[24] S. Maghous, L. Dormieux, and J.F. Barthélémy. Micromechanical approach to the strength properties of frictional geomaterials. *European Journal of Mechanics A/Solid*, 28:179–188, 2009.

[25] V. Monchiet and G. Bonnet. A Gurson-type model accounting for void size effects. *International Journal of Solids and Structures*, 50:320–327, 2013.

[26] V. Monchiet, E. Charkaluk, and D. Kondo. Macroscopic yield criteria for ductile materials containing spheroidal voids: An eshelby-like velocity fields approach. *Mechanics of Materials*, 72:1–18, 2014.

[27] V. Monchiet and D. Kondo. Combined voids size and shape effects on the macroscopic criterion of ductile nanoporous materials. *International Journal of Plasticity*, 43:20–41, 2013.

[28] F. Pastor and D. Kondo. Limit analysis and lower/upper bounds to the macroscopic criterion of drucker-prager materials with spheroidal voids. *Comptes Rendus Mecanique*, 342:96–105, 2014.

[29] F. Pastor, D. Kondo, and J Pastor. 3d-fem formulations of limit analysis methods for porous pressure-sensitive materials. *Int. J. Numer. Meth. Engng*, DOI: 10.1002/nme.4527, 2013.

[30] J. Pastor, P. Thoré, and F. Pastor. Limit analysis and numerical modeling of spherically porous solids with coulomb and drucker-prager matrices. *Journal of Computational and Applied Mathematics*, 234:2162–2174, 2010.

[31] J. Salençon. An introduction to the yield theory and its applications to soil mechanics. *European Journal of Mechanics A/Solids*, 9(5):477–500, 1990.

[32] Valentina A. Salomoni and Riccardo Fincato. 3d subsidence analyses above gas reservoirs accounting for an unconventional plasticity model. *International Journal for Numerical and Analytical Methods in Geomechanics*, 36(8):959–976, 2012.

[33] B. A. Schrefler, L. Simoni, Li Xikui, and O. C. Zienkiewicz. *Mechanics of Partially Saturated Porous Media*, pages 169–209. Springer Vienna, Vienna, 1990.

[34] W. Q. Shen, E. Lanoye, L. Dormieux, and D. Kondo. Homogenization of saturated double porous media with eshelby-like velocity field. *Acta Geophysica.*, 62(5):1146–1162, 2014.

[35] W. Q. Shen and J. F. Shao. An elastic-plastic model for porous rocks with two populations of voids. *Computers and Geotechnics*, 76:194–200, 2016.

[36] W. Q. Shen and J. F. Shao. An incremental micro-macro model for porous geomaterials with double porosity and inclusion. *International Journal of Plasticity*, 83:37–54, 2016.

[37] W. Q. Shen, J. Zhang, J. F. Shao, and D Kondo. Approximate macroscopic yield criteria for drucker-prager type solids with spheroidal voids. *International Journal of Plasticity*, 99:221–247, 2017.

[38] W.Q. Shen, Z. He, L. Dormieux, and D. Kondo. Effective strength of saturated double porous media with a drucker-prager solid phase. *Int. J. Numer. Anal. Meth. Geomech.*, 38:281–296, 2014.

[39] W.Q. Shen, D. Kondo, L. Dormieux, and J.F. Shao. A closed-form three scale model for ductile rocks with a plastically compressible porous matrix. *Mechanics of Materials*, 59:73–86, 2013.

[40] W.Q. Shen, A. Oueslati, and G. De Saxce. Macroscopic criterion for ductile porous materials based on a statically admissible microscopic stress field. *International Journal of Plasticity*, 70:60–76, 2015.

[41] W.Q. Shen, J.F. Shao, D. Kondo, and B Gatmiri. A micro-macro model for clayey rocks with a plastic compressible porous matrix. *International Journal of Plasticity*, 36:64–85, 2012.

[42] W.Q. Shen, J.F. Shao, A. Oueslati, G. De Saxcé, and J. Zhang. An approximate strength criterion of porous materials with a pressure sensitive and tension-compression asymmetry matrix. *International Journal of Engineering Science*, 132:1 – 15, 2018.

[43] L. Simoni, V. Salomoni, and B.A. Schrefler. Elastoplastic subsidence models with and without capillary effects. *Computer Methods in Applied Mechanics and Engineering*, 171(3):491 – 502, 1999.

[44] P. Thoré, F. Pastor, and J. Pastor. Hollow sphere models, conic programming and third stress invariant. *European Journal of Mechanics A/Solids*, 30:63–71, 2011.

[45] P. Thoré, F. Pastor, J. Pastor, and D. Kondo. Closed-form solutions for the hollow sphere model with coulomb and drucker-prager materials under isotropic loadings. *C. R. Mecanique*, 337:260–267, 2009.

[46] M. Trillat and J. Pastor. Limit analysis and Gurson's model. *Eur. J. of Mechanics*, 24:800–819, 2005.

[47] V. Tvergaard. Influence of voids on shear bands instabilities under plane strain conditions. *Int. J. Fracture*, 17:389–407, 1981.

[48] V. Tvergaard. Material failure by void coalescence in localized shear bands. *Int. J. Solids Structures*, 18(8):659–672, 1982.

[49] P.-G. Vincent, Y. Monerie, and Suquet P. Ductile damage of porous materials with two populations of voids. *C.R.Mecanique*, 336:245–259, 2008.

[50] P.-G. Vincent, Y. Monerie, and Suquet P. Porous materials with two populations of voids under internal pressure: I. instantaneous constitutive relations. *Int J Solids Struct*, 46:480–506, 2009.

[51] S.Y. Xie and J.F. Shao. Experimental investigation and poroplastic modelling of saturated porous geomaterials. *International Journal of Plasticity*, 39:27 – 45, 2012.

[52] Ismail Yurtdas, Nicolas Burlion, and Frédéric Skoczylas. Triaxial mechanical behaviour of mortar: Effects of drying. *Cement and Concrete Research*, 34(7):1131 – 1143, 2004.